Monthly Notices
of the
ROYAL ASTRONOMICAL SOCIETY

MNRAS **475,** 193–219 (2018)
Advance Access publication 2017 December 6

doi:10.1093/mnras/stx3136

The Foundation Supernova Survey: motivation, design, implementation, and first data release

Ryan J. Foley,[1]★ Daniel Scolnic,[2] Armin Rest,[3] S. W. Jha,[4] Y.-C. Pan,[1] A. G. Riess,[5,3] P. Challis,[6] K. C. Chambers,[7] D. A. Coulter,[1] K. G. Dettman,[4] M. M. Foley,[8] O. D. Fox,[3] M. E. Huber,[7] D. O. Jones,[1] C. D. Kilpatrick,[1] R. P. Kirshner,[6,9] A. S. B. Schultz,[7] M. R. Siebert,[1] H. A. Flewelling,[7] B. Gibson,[7] E. A. Magnier,[7] J. A. Miller,[10] N. Primak,[7] S. J. Smartt,[11] K. W. Smith,[11] R. J. Wainscoat,[7] C. Waters[7] and M. Willman[7]

[1]*Department of Astronomy and Astrophysics, University of California, Santa Cruz, CA 95064, USA*
[2]*Kavli Institute for Cosmological Physics, The University of Chicago, Chicago, IL 60637, USA*
[3]*Space Telescope Science Institute, 3700 San Martin Drive, Baltimore, MD 21218, USA*
[4]*Department of Physics and Astronomy, Rutgers, The State University of New Jersey, 136 Frelinghuysen Road, Piscataway, NJ 08854, USA*
[5]*Department of Physics and Astronomy, Johns Hopkins University, Baltimore, MD 21218, USA*
[6]*Harvard College Observatory, Harvard University, 60 Garden Street, Cambridge MA 02138, USA*
[7]*Institute for Astronomy, University of Hawaii, 2680 Woodlawn Drive, Honolulu, HI 96822, USA*
[8]*Department of Physics, University of Notre Dame, Notre Dame, IN 46556, USA*
[9]*Gordon and Betty Moore Foundation, 1661 Page Mill Road, Palo Alto, CA 94304, USA*
[10]*Astronomy Department, University of Illinois at Urbana–Champaign, 1002 W. Green Street, Urbana, IL 61801, USA*
[11]*Astrophysics Research Centre, School of Mathematics and Physics, Queen's University Belfast, Belfast BT7 1NN, UK*

Accepted 2017 November 6. Received 2017 November 3; in original form 2017 September 4

ABSTRACT

The Foundation Supernova Survey aims to provide a large, high-fidelity, homogeneous, and precisely calibrated low-redshift Type Ia supernova (SN Ia) sample for cosmology. The calibration of the current low-redshift SN sample is the largest component of systematic uncertainties for SN cosmology, and new data are necessary to make progress. We present the motivation, survey design, observation strategy, implementation, and first results for the Foundation Supernova Survey. We are using the Pan-STARRS telescope to obtain photometry for up to 800 SNe Ia at $z \lesssim 0.1$. This strategy has several unique advantages: (1) the Pan-STARRS system is a superbly calibrated telescopic system, (2) Pan-STARRS has observed 3/4 of the sky in $grizy_{\rm P1}$ making future template observations unnecessary, (3) we have a well-tested data-reduction pipeline, and (4) we have observed ∼3000 high-redshift SNe Ia on this system. Here, we present our initial sample of 225 SN Ia $griz_{\rm P1}$ light curves, of which 180 pass all criteria for inclusion in a cosmological sample. The Foundation Supernova Survey already contains more cosmologically useful SNe Ia than all other published low-redshift SN Ia samples combined. We expect that the systematic uncertainties for the Foundation Supernova Sample will be two to three times smaller than other low-redshift samples. We find that our cosmologically useful sample has an intrinsic scatter of 0.111 mag, smaller than other low-redshift samples. We perform detailed simulations showing that simply replacing the current low-redshift SN Ia sample with an equally sized Foundation sample will improve the precision on the dark energy equation-of-state parameter by 35 per cent, and the dark energy figure of merit by 72 per cent.

Key words: surveys – supernovae: general – dark energy – distance scale – cosmology: observations.

★ E-mail: foley@ucsc.edu

1 INTRODUCTION

Observations of Type Ia supernovae (SNe Ia) led to the discovery that the Universe's expansion is currently accelerating (Riess et al. 1998; Perlmutter et al. 1999). SNe Ia continue to be a mature and important cosmological tool (e.g. Suzuki et al. 2012; Betoule et al. 2014; Rest et al. 2014; Jones et al. 2017; Scolnic et al. 2017). Further observations of SNe Ia will be critical to improve an understanding of the nature of dark energy, perhaps the most puzzling open problem in all of physics.

Several observational methods have been employed to address this problem. This multiprobe approach has dramatically improved our ability to constrain dark energy parameters such as its equation of state, $w = P/\rho c^2$, where P is its pressure and ρ is its density, and any evolution of w with redshift or cosmic time. Although in many ways the simplest explanation consistent with current observations is that dark energy is a cosmological constant with $w = -1$, recent results hint at a possible deviation from this (e.g. Planck Collaboration XVI 2014; Rest et al. 2014). At the very least, this demonstrates that there is currently no definitive answer to exactly what is driving the Universe's accelerated expansion, and new data and analyses are required to make progress. To that end, SNe Ia are still an exquisite tool with which we can precisely measure the expansion history of the Universe.

Since dark energy may evolve over cosmic time, one can describe a more general parametrization of the equation-of-state parameter,

$$w(a) = P(a)/\rho(a)c^2 \quad (1)$$

$$= w_0 + (1 - a)w_a, \quad (2)$$

where $a = (1 + z)^{-1}$ is the scale factor of the Universe, w_0 is the current equation-of-state parameter of dark energy, and w_a parameterizes the evolution of the equation-of-state parameter (see e.g. Chevallier & Polarski 2001; Linder 2003). In order to quantify our knowledge (or ignorance) of dark energy, the Dark Energy Task Force defined a figure of merit (FoM) which is equal to the inverse of the area enclosed within the 95 per cent confidence contour in the w_0–w_a plane (and equivalent to the inverse of the square root of the determinant of the covariance matrix for w_0 and w_a; Albrecht et al. 2006; Wang 2008). With this choice, larger FoMs indicate increasing knowledge of dark energy. As a point of reference, a recent analysis combining multiple probes had an FoM of 32.6 (Alam et al. 2017).

Another fundamental cosmological parameter measurable with observations of SNe Ia is the Hubble constant, H_0. The Hubble constant is also critically related to the age of the Universe and indirectly constrains w (Hu 2005). Over the last decade, the uncertainty on the Hubble constant has been significantly reduced (e.g. Riess et al. 2009, 2011; Freedman et al. 2012, see Freedman & Madore 2010 for a recent review). The most recent progress in constraining the Hubble constant has reduced the uncertainty to 2.4 per cent (Riess et al. 2016). Much of this success has been the result of linking measurements of precise, abundant, but relatively faint distance indicators such as Cepheid variables with measurements of precise, less frequent, and relatively luminous distance indicators such as SNe Ia. Recently, direct measurements of H_0 seem in conflict (at the 3.4σ level) with the inferred values derived from indirect techniques such as combining measurements of the cosmic microwave background (CMB) with large-scale structure (Planck Collaboration XIII 2016; Alam et al. 2017). This tension could be the result of subtle systematic uncertainties in the various measurements, but could also point to interesting new physics such as an additional relativistic species akin to neutrinos, but distinct from the known members of that family.

At this point, we have amassed enough SNe that the precision for w is not limited by statistical precision, but rather systematic floors in our ability to measure the distances to SNe Ia prevent further progress.

Currently, the largest systematic uncertainty for high-z SN cosmology is photometric calibration (Conley et al. 2011; Betoule et al. 2014; Scolnic et al. 2014b, 2017). Cosmological constraints from SNe Ia are derived by comparing the distances of low- to high-z SNe, with the low-z sample providing an 'anchor' to the high-z sample. At the moment, the heterogeneous low-z SN Ia sample is a larger source of calibration uncertainty than the high-z samples, and all other individual systematic uncertainties. Additionally, the high-z samples are now much larger than the low-z sample (e.g. Scolnic et al. 2017), meaning that the statistical weight of each low-z SN is currently larger than each high-z SN. Any work on high-z samples will have a marginal effect on w until we improve the low-z sample (Astier et al. 2014; Spergel et al. 2015).

Here, we present the strategy, implementation, and first results for the Foundation Supernova Survey. The Foundation Supernova Survey is designed to replace the current low-z ($z < 0.1$) SN Ia sample with a large, homogeneous, high-fidelity sample which can be used as the low-z anchor (and *foundation*) for future cosmological analyses. This sample will address the largest uncertainty in SN cosmology, significantly reducing the total uncertainty for w. The Foundation Supernova Survey will fulfil a large portion, and perhaps all, of the *WFIRST* low-z sample requirement (Spergel et al. 2015). Since the Large Synoptic Survey Telescope (LSST) will saturate at $m \approx 17$ mag, the Foundation Supernova Survey may be the fundamental low-z SN Ia sample, especially for measurements of H_0, for at least a decade.

This manuscript is structured as follows. Section 2 describes the overall survey requirements, strategy, and design choices; Section 3 presents observations and data reduction for our initial sample of SNe observed in the first few months of the survey; Section 5 presents our initial results; and Section 6 discusses our future goals and possible improvements.

2 SURVEY DESIGN

2.1 Motivation

Current SN Ia cosmology analyses (e.g. Rest et al. 2014) use ∼200 low-z SNe Ia from six different low-z surveys, each on a different photometric system with different cadences and systematic errors. The heroic effort of creating the current low-z SN Ia sample was performed over more than two decades, and some of these data were critical in the original detection of the accelerating universe.

The Rest et al. (2014) analysis, which used a particularly large low-z sample (larger than e.g. Betoule et al. 2014), included samples from the following surveys: *Calán/Tololo* (16 SNe after various quality cuts, including a redshift cut to only include SNe in the Hubble flow [$z > 0.015$]; mostly CTIO 0.9-m + Tek1, Tek2, Tek3, Tek IV, TI2, TI3; Hamuy et al. 1996), *CfA1* (5 SNe; mostly 1.2-m FLWO + thick/thin CCDs; Riess et al. 1999), *CfA2* (19 SNe; 1.2-m + Andycam, 4Shooter; Jha et al. 2006), *CfA3* (85 SNe; 1.2-m + 4Shooter, Minicam, and Keplercam; Hicken et al. 2009a), *CfA4* (43 SNe; 1.2-m + Keplercam; Hicken et al. 2012), *CSP* (45 SNe; Swope + SITe3; templates from du Pont; Contreras et al. 2010), and 8 *'other SNe'* included by Jha et al. (2006). Even without considering multiple filter systems for a given telescope/camera,

the low-z SN Ia sample is constructed from >13 systems, with the largest and second-largest homogeneous samples being the 1.2-m/Keplercam (used for part of CfA3 and CfA4, respectively) and 1.2-m/4Shooter systems with 93 and 32 SNe Ia, respectively. One could also include other surveys such as *LOSS* (mostly KAIT + Apogee, Apogee2, FLI; Ganeshalingam et al. 2010), but that only increases the inhomogeneity.

The cosmological systematic uncertainty associated with this heterogeneous low-z sample is perhaps best demonstrated by the shift in the measured value of w when we exclude a survey. When Scolnic et al. (2014b) excluded the CSP sample, w shifted by -0.021 even when combining with CMB and baryon acoustic oscillation (BAO) data. On the other hand, excluding CfA1, CfA2, and the 'other' SNe shifted w by $+0.022$. This >4 per cent overall shift is larger than that expected from the increased statistical uncertainty from removing the samples and an indication of a large systematic bias – but it does not fully capture our ignorance. There remain fundamental and irreducible systematic uncertainties associated with the data where the cameras, filters, *and even telescopes* no longer exist.

Additionally, the calibration errors from the many different low-z samples propagate through the analysis in multiple ways as we fit *all* SN Ia light curves using models determined primarily from the low-z SNe. These systematic uncertainties have only begun to be unravelled (Mosher et al. 2014) and likely result in a moderate bias in our measurement of w.

Because the older surveys did not always start monitoring the SN before peak brightness, did not always have sufficient filter coverage and/or cadence, and observed many SNe Ia that were not in the Hubble flow ($z > 0.015$), only 45 per cent of the observed low-z SNe are included in current analyses. Many records from 20 yr ago are now lost, and therefore we cannot precisely model the selection bias for the current sample. Since past low-z samples are a subset of the SNe discovered during that era, and most low-z SN surveys targeted large galaxies, there are well-known selection biases (Scolnic et al. 2014a) in the colour and luminosity distributions of the sample. These biases also propagate into the systematic uncertainty through the SN colour model, the host galaxy dependence, and the selection bias itself.

We have concluded that the current heterogeneous low-z SN Ia sample is limiting current cosmological analyses. Although one can make some modest improvements in the sample with great effort (Scolnic et al. 2015), ultimately, the sample must be replaced to break through the current systematic floors. Fortunately, the SN discovery rate, particularly for SNe before maximum brightness, has increased significantly over the past few years (e.g. Gal-Yam et al. 2013), and a sufficient number of SNe Ia are discovered to completely replace the number of SNe Ia in the low-z sample within 1–2 yr.

2.2 Telescopic system requirements

When considering replacing the low-z SN sample, one must identify the limitations of the current sample. The photometric calibration is clearly the largest hurdle, which can be separated into two main components: the characterization of a given system and placing that system on a physical scale.

If all potential calibration systematic uncertainties are properly assessed for all surveys, one could combine all data to 'average' any potential biases in a single survey. However, in practice, some uncertainties are highly correlated between systems (such as absolute flux calibration) and some systematic uncertainties may be underestimated (Scolnic et al. 2015). As such, one must be careful in choosing a specific sample for inclusion in an analysis.

Although we make no specific recommendations for inclusion/exclusion here, we note that every additional telescope, camera, and/or filter will result in increased calibration uncertainty. While many different systems may reduce the overall systematic uncertainty, a practical place to start is to calibrate a single telescopic system as well as possible.

To do this, the telescopic system should be externally well calibrated and self-consistent. That is, the absolute and relative photometric uncertainty of the system should be minimized. One can significantly improve the relative photometric calibration by linking all SN fields together through overlapping observations. This 'übercalibration' has been performed for the large-footprint Sloan Digital Sky Survey (SDSS) and Pan-STARRS1 (PS1) surveys (Padmanabhan et al. 2008; Schlafly et al. 2012), but is difficult to do with any small field-of-view camera. Moreover, multiple observations of the sky spread out in time improves this calibration significantly. Precise absolute calibration can be obtained by observing spectrophotometric standard stars.

Next, the filter response functions should be precisely measured. Ideally, this is done with a tunable laser diode or monochromator to measure the full system throughput as a function of wavelength (e.g. Rheault et al. 2010; Stubbs & Tonry 2012).

Finally, an ideal system should have already observed a large *high-redshift* SN Ia sample. Such a sample would allow a measurement of cosmological samples using a single telescopic system, reducing the number of free parameters in the systematic error budget to the minimal case.

Of all available telescopic systems, only PS1 has all desired characteristics. It is therefore an ideal platform upon which one could construct a new low-z SN Ia sample.

2.3 The Pan-STARRS-1 System

The PS1 system is a high-etendue wide-field imaging system, designed for dedicated survey observations. The system is installed on the peak of Haleakala on the island of Maui in the Hawaiian island chain. We provide below a terse summary of the PS1 survey instrumentation. A more complete description of the PS1 system, both hardware and software, is provided by Kaiser et al. (2010), Chambers et al. (2016), and references therein.

The PS1 optical design (Hodapp et al. 2004) uses a 1.8 m diameter $f/4.4$ primary mirror, and a 0.9 m secondary. The telescope delivers images with low distortion over a field diameter of 3.3 deg. The 1.4 Gigapixel PS1 imager (Tonry & Onaka 2009) comprises a total of 60 4800 × 4800 pixel detectors, with 10 μm pixels that subtend 0.258 arcsec. The detectors are back-illuminated CCDs manufactured by Lincoln Laboratory, which are read out using a StarGrasp CCD controller in 7 s for a full unbinned image. Initial performance assessments are presented in Onaka et al. (2008).

The PS1 observations are obtained through a set of five broadband filters, which we have designated as $g_{\rm P1}$, $r_{\rm P1}$, $i_{\rm P1}$, $z_{\rm P1}$, and $y_{\rm P1}$ ($grizy_{\rm P1}$). The PS1 system also has a wide *gri*-composite filter $w_{\rm P1}$, which is not currently used by our survey. Instrumental response functions for the PS1 filters have been measured by Tonry et al. (2012).

PS1 has unique and important characteristics for building a low-z SN Ia sample. (1) The telescope has already observed 3/4 (3π) of the sky in five filters. (2) PS1 has a superb relative photometric calibration down to a few mmag (Schlafly et al. 2012; Magnier et al. 2013). Because of its excellent calibration, PS1 has been used

to re-calibrate SDSS (Finkbeiner et al. 2016). (3) PS1 has one of the best-measured instrument response functions, making SN photometry extremely precise (Stubbs et al. 2010; Magnier et al. 2016). (4) There already exists a very large PS1 high-z SN Ia sample ($\sim$400 spectroscopically confirmed SNe Ia; Rest et al. 2014; Scolnic et al. 2017). (5) Because of our familiarity with PS1, we can use our robustly tested and optimized pipeline to quickly produce light curves from our newly acquired data. We detail these advantages below.

(i) *Sky coverage*: the PS1 3π survey was completed at the beginning of 2014 (see Chambers et al. 2016 for a description of the 3π survey strategy). Roughly 12 images of every position north of -30 declination were observed in five filters (60 total images). The stacked images are roughly as deep as SDSS in *gr*, but as much as 0.5–1 mag deeper in *iz*, with typically better seeing (Metcalfe et al. 2013). Multiple images, each providing independent measurements, improve the absolute calibration and reduce cosmetic defects such as bad pixels, chip gaps, satellite trails, etc. The PS1 Science Consortium has publicly released the stacked sky images and catalogues through the Space Telescope Science Institute (STScI), and the data can be accessed through MAST, the Mikulski Archive for Space Telescopes.[1]

The field for any SN that PS1 can observe at relatively low airmass has already been observed as part of the 3π survey. This immediately provides photometric zero-points and templates for all new SNe Ia. Without the need for templates after the SN has faded, the amount of telescope time is reduced. But more importantly, final photometry can be measured immediately; one does not need to wait a year (or longer) for the SN to fade before getting templates.

(ii) *Well-calibrated photometric system*: the PS1 system already has a calibration that is significantly more uniform than any low-z survey. In fact, the PS1 calibration is at least as good as SDSS, where PS1 images can now be used to correct SDSS photometry (Finkbeiner et al. 2016). The PS1 calibration will keep improving in the coming years as PS1 continues to observe and calibration methodology improves. By linking to the 3π data, SN photometry can be calibrated to $<$5 mmag precision.

This is in contrast to other low-z surveys, which observe Landolt or other spectrophotometric standard stars during photometric nights, and then convert those magnitudes to the standard AB system to determine photometric zero-points.

(iii) *Precise and accurate instrument response*: an accurate instrument response function is essential for the spectral-model fitting needed to compare SNe Ia at different redshifts. The state-of-the art method to measure the instrument response function is to use an NIST-calibrated photodiode in combination with a tunable laser system to pass a known amount of light through the entire telescope system in small wavelength increments (Stubbs et al. 2007, 2010; Stubbs & Tonry 2012).

This is a relatively technical, time-intensive, and expensive measurement. Even with infinite resources, we would be unable to make this measurement for the majority of the current low-z sample – for many, the cameras have been de-commissioned and the filters have degraded with time.

A very large amount of person power, money, and telescope time has already been put into characterizing the PS1 system using a tunable laser, and as a result, it has one of the best-measured instrument response functions with sub-nm precision for the effective filter wavelengths.

[1] http://panstarrs.stsci.edu/

Furthermore, repeated PS1 imaging of 10 Medium-Deep fields (MDFs) over 4.5 yr provides hundreds of measurements of thousands of stars to determine if the system is evolving with time. Thus far, we have constrained any evolution to $<$3 mmag over the first two years of the PS1 survey (Scolnic et al. 2017).

Although significant effort has already been put into producing the current PS1 calibration, it can be further improved. One of the greatest advantages of the PS1 survey is that it covers such a large portion of the sky, including the majority of *HST* Calspec standards (with a magnitude range of 12–17; Bohlin 1996). The Calspec standards are observed by *HST*, an extremely stable system where calibration systematic uncertainties are small and well understood. For each star, there is a stellar atmosphere model, which can be used to determine the agreement between the observations and theoretical expectations. By comparing different Calspec stars, it has been shown that the sample is internally consistent (Scolnic et al., in preparation). The Calspec standards define the absolute flux scale of the PS1 system, and the Foundation sample will be the first low-z sample to be tied directly to the Calspec standards, completely removing the dependence on Landolt standards, Vega, and other calibrators, and thus removing a step in our calibration procedure. Furthermore, because PS1 has been cross-calibrated to other high-z surveys (Scolnic et al. 2015), any future improvement in the calibration of these surveys can directly benefit the calibration of the PS1 system.

Continued PS1 observations will continue to measure any potential temporal evolution of the system. Additionally, several new *HST* standard stars were specifically chosen to be in the MDFs (Narayan et al. 2016b), meaning that for a subset of standard stars, there will be hundreds of observations.

(iv) *Low- and high-z samples on the same photometric system*: Having a large set of both low- and high-z SN Ia observations from a single telescopic system is highly advantageous. A cosmological analysis of such a data set will remove all cross-system calibration systematic errors. As different surveys observe SNe in different redshift regimes, calibration systematics between surveys potentially introduce large cosmological biases. The total calibration systematic uncertainty for w is currently 4.5 per cent. This single systematic uncertainty is almost as large as the entire statistical error for the recent PS1 analysis (5.0 per cent; Rest et al. 2014; Scolnic et al. 2014b).

Calibration has been significantly improved over the last 10 yr for the high-z samples, and their cross-calibration has greatly improved their overall calibration (Betoule et al. 2014; Scolnic et al. 2017). However, the low-z calibration is only loosely tied to the high-z calibration, and a path for improving the current sample is not obvious as the calibration systems used for many of the low-z surveys were not measured using the current state-of-the-art techniques (Scolnic et al. 2015). Since some systems have been decommissioned, the path to further improvement in those cases is not clear.

(v) *Established data reduction pipeline:* to produce the light curves for the high-z PS1 SN Ia sample, Rest et al. (2014) adapted the well-tested `photpipe` data reduction pipeline (Rest et al. 2005) to work with PS1 data. After basic data processing by the PS1 Image Processing Pipeline (IPP; Magnier 2006; Magnier et al. 2013; Waters et al. 2016), `photpipe` further reduces the data, performs photometry, and generates publication-quality SN light curves. We have made some additional minor modifications to this pipeline to process Foundation data. We further describe the data reduction pipeline in Section 3.

Although we are still working to improve this pipeline further (e.g. implementing a scene-modelling photometry package;

Holtzman et al. 2008), its existence means that any SN observations with PS1 can immediately be converted into publication-quality photometry *with the first SN image*. Unlike other low-z surveys, using PS1 avoids the need to expend person power on writing or adapting a data reduction pipeline and decreases the time between data acquisition and publication of the Foundation sample.

In summary, the PS1 system fulfils all telescopic system requirements (Section 2.2) and is ideal for generating a new low-z SN Ia sample for cosmology.

2.4 Foundation Supernova Survey strategy

Having determined that the current low-z SN Ia sample is impeding progress in understanding dark energy and that the PS1 system is ideal for improving the sample, we now describe the Foundation Supernova Survey strategy.

The Foundation Supernova Survey aims to observe a large sample of low-z SNe Ia with PS1. By observing with PS1, the Foundation sample will be on one of the best-calibrated photometric systems available, providing a calibration accurate to a few mmag. Furthermore, at the end of the survey, the Foundation Supernova sample will be both large enough and sufficiently calibrated that adding existing low-z samples to a cosmological analysis will typically provide little improvement in the resulting measurements.

The Foundation Supernova Survey is a follow-up survey. The Pan-STARRS1 Science Consortium finished the 3π sky survey in 2014, and since then the PS1 telescope has been running a wide-area survey (mostly around the ecliptic) focused on a near-earth object (NEO) search. Around 90 per cent of the time is dedicated to this survey which takes four images each night using $w_{\rm P1}$ in dark time and combinations of $i_{\rm P1}$ and $z_{\rm P1}$ in bright moon time. These data are used to discover SNe by the Pan-STARRS Survey for Transients (PSST; Huber et al. 2015; Polshaw et al. 2015; Nicholl et al. 2016), with more than 3000 SN candidates reported to the IAU Transient Name Server in 2016. The cadence and filter deployment of the NEO survey data is not adequate to produce SN light curves sufficient for measuring distances. Instead the Foundation Supernova Survey triggers PS1 to take follow-up observations on known, low-z SNe, but does use PSST images to supplement our targeted observations.

2.4.1 Target selection

To avoid biases related with targeted SN surveys, we primarily draw our sample from untargeted surveys. At the time of publication, the majority of (announced) bright ($m < 17$ mag) and faint ($17 < m < 21$ mag) nearby SNe are discovered by the All-Sky Automated Survey for Supernovae (ASAS-SN; Shappee et al. 2014); see also Holoien et al. 2017a,b and PS1 through the Pan-STARRS Survey for Transients (PSST; Huber et al. 2015), respectively.[2] These two surveys are the initial (or secondary, independent) discoverers of 40 per cent (41 per cent) and 21 per cent (45 per cent) of our full sample, respectively.

However, we do not exclusively observe SNe discovered by these surveys. Other surveys are similar in cadence and depth and, for purposes of simulating efficiencies, can be treated as extensions of these surveys. Moreover, other surveys, including targeted surveys, can discover SNe that ASAS-SN and/or PSST would have discovered if that survey did not exist. Removing these objects from our selection could also introduce biases.

To be selected for full follow-up observations, an SN must (1) be in the Hubble flow ($z > 0.015$) but close enough such that we obtain high-signal-to-noise ratio (S/N) photometric observations with minimal Malmquist bias ($z \lesssim 0.08$) or close enough where measuring a Cepheid or Tip of the Red Giant Branch (TRGB) distance is feasible ($D \lesssim 40$ Mpc), (2) have relatively low Milky Way reddening ($E(B-V)_{\rm MW} < 0.2$ mag), (3) be at $\delta > 30^\circ$ to fall into the 3π footprint, (4) be observable by PS1 for at least 45 d, and (5) be spectroscopically confirmed as an SN Ia where our first observation can be scheduled before maximum brightness.

As we require a spectroscopic classification for a full set of follow-up observations, we are often reliant on public classifications. Although we have spectroscopic follow-up time (primarily with SOAR, SALT, and the KPNO 4-m telescope), other classifications are often used for selection. When possible, we obtain a spectrum of every Foundation SN to confirm its classification, measure spectral properties, and estimate the phase of our first photometric observation.

To avoid significant biases related to spectroscopic classification, we obtain 'snapshot' observations of potential Foundation SNe before classification. These observations consist of a single epoch of $gri_{\rm P1}$ data. SNe for which there is a (sufficiently deep) non-detection within 15 d of discovery, fulfil other requirements, and are associated with a $z \lesssim 0.08$ galaxy (including photometric redshift estimates), and where we think that a public classification, including from our spectroscopic resources, will plausibly occur within one week of discovery are observed. The last requirement results in observing any reasonable candidate discovered up to a week before one of our classical spectroscopic telescope nights (with considerations for declination when our resources are southern), any $m < 17$ mag SN discovered after full and before new moon, and any $m < 15$ mag SN.

We do not perform any additional observations until a classification spectrum is obtained. If no classification spectrum is obtained within a week, we discontinue all observations. If the spectrum indicates that the object is not an SN Ia, it is not within our redshift range, or our snapshot observation was not before maximum brightness, we discontinue all observations.

At the current rate, roughly 300 appropriate SNe Ia are discovered per year. The main hurdle is spectroscopic classification. On a recent SOAR night, we were able to observe 17 SNe and classify 10 SNe, of which 6 are now included in the Foundation sample (Pan et al. 2015b). Even if only one-third of all SNe observed are ultimately included in the Foundation sample, we should be able to obtain spectra of $\sim$150 Foundation SNe per year with two 4-m nights per month. Such follow-up time has been awarded for several semesters (PI Foley: NOAO Programmes 2015A-0253, 2015B-0313, 2017B-0058, 2017B-0169; Lick Programme 2017A_S011; Keck Programme 2017A_U079; PI Jha: SALT Programmes 2015-1-MLT-002, 2016-1-MLT-007, 2017-1-MLT-002).

We will also make an effort to carefully observe all potential Cepheid/TRGB SNe Ia at higher cadence (and shorter exposure times to avoid saturation and maintain a constant open-shutter time). Although this sample will initially be small, we should be able to observe $\sim$2 Cepheid/TRGB-SN calibrators per year. This rate is relatively small, but current H_0 analyses use only 19 Cepheid SNe Ia (Riess et al. 2016), and we will be able to contribute a large increase in this sample in a few years of observations. Having the Cepheid SNe and the Hubble-flow SNe on the same system will remove a large systematic uncertainty for the measurement of H_0. We may

[2] See https://wis-tns.weizmann.ac.il/stats-maps for discovery statistics.

continue to observe Cepheid/TRGB SNe Ia after the conclusion of the Foundation Supernova Survey, and increasing statistics now is important because of the low rate.

2.4.2 *Exposure time and cadence*

The primary driver for the exposure time and cadence of the Foundation Supernova Survey is the statistical distance uncertainty, which we would like to be smaller than the intrinsic scatter in the sample, $\sigma_{\rm int}$. While different studies have found a range of $\sigma_{\rm int}$ (e.g. Hicken et al. 2009b; Betoule et al. 2014; Scolnic et al. 2015), most have $0.10 < \sigma_{\rm int} < 0.17$ mag. We therefore aim to have a statistical distance uncertainty of <0.10 mag.

The first consideration for the distance uncertainty is an adequate cadence to properly measure the peak brightness and light-curve shape for each SN. At a minimum, this requires three epochs (before peak, near peak, and at $t \gtrsim 15$ d). We performed simulations that suggest that such a cadence, if performed with sufficiently high S/N observations is sufficient for measuring the peak brightness and light-curve shape of an SN Ia. However, this is an optimistic scenario, and cautious observers would generally prefer more observations.

If we adequately measure the peak of the light curve and the light-curve shape, the dominant term in the distance uncertainty is the colour uncertainty. The intrinsic colour variation for a given light-curve shape is of the order of 0.03 mag (Scolnic & Kessler 2016; Mandel et al. 2017), and therefore we would like to reach this level of precision. Additionally, the effect of the colour uncertainty on the distance is roughly three times that of the uncertainty on peak brightness, and to reach a distance uncertainty of 0.10 mag, we must measure the SN colour to $\lesssim$0.03 mag.

The colour precision is roughly determined by the overall S/N of all light-curve points (assuming roughly similar S/N in each band). Therefore, there is a degeneracy between the exposure time of an individual epoch and the number of epochs for a light curve. Here, we examine the optimal values given some constraints.

Our first constraint is that we require ≥3 epochs to constrain the peak brightness and light-curve shape. Secondly, the PS1 camera, GPC1, has a read-out time of 7 s. To avoid excessive overhead and to make the images sky-noise dominated (rather than read-noise dominated), we have limited our exposure times to be a minimum of 15 s. In a 15-s exposure, SNe with $griz_{\rm P1}$ magnitudes of 18 (20) typically have S/N = 44, 54, 52, and 40 (10, 12, 11, and 8), respectively. If observations are set to the minimum exposure time, the light curves will have sufficient S/N to measure the colour to our desired value in five epochs.

However, there are other uncertainties related to the number of epochs, including the zero-point uncertainty of local stars, which we find is typically <5 mmag. This, combined with potential catastrophic events (such as cosmic ray hits or satellite trails), makes a larger number of epochs desirable. As a result, we aim to obtain the minimum number of epochs at the shortest exposure time where the combination results in a colour uncertainty below our goal. Having more epochs is also likely more interesting for understanding the physics of SN Ia progenitors and explosions and will make our light curves more useful for light-curve training. Our simulations have shown that roughly seven epochs provide the optimal light curves. The seven epochs could be scheduled such that there are different-sized gaps between epochs at different phases of the light curve. For instance, one might want to observe nightly near peak and every 10 d later. However, such a cadence is difficult to obtain in practice. A shorter cadence is difficult to consistently achieve given typical stretches of bad weather, where the telescope can have gaps of >3 d. It also places additional stress on the telescope scheduling and requires more effort. We chose an average cadence around peak of 5 d for simplicity and to roughly match the cadences of the SDSS and SNLS surveys. We chose our final observation to be at $\gtrsim$35 d after peak to measure the late-time colour (which has been shown to be a good indicator of dust reddening; Lira 1996). The nominal sequence is then −5, 0, 5, 10, 18, 26, and 35 d relative to peak.

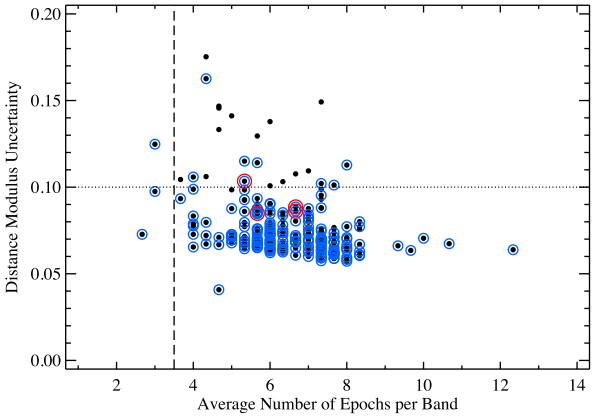

Figure 1. Distance modulus uncertainty as a function of average number of epochs observed per band for the Foundation sample (black dots). Blue circles indicate SNe that pass all criteria for inclusion in our cosmology sample (Section 5.3) *except* for the requirement that there be an average of >3.6 epochs per band (in $gri_{\rm P1}$) and that the first epoch be earlier than 7 d after peak brightness. The red circles indicate SNe that pass all criteria *except* that the first epoch be earlier than a week past peak brightness. The dotted horizontal line represents our goal of a 0.10 mag distance modulus uncertainty. The vertical dashed line represents the average number of epochs necessary for inclusion in the cosmology sample. Objects with more epochs have typical distance uncertainties of ≤0.10 mag.

For this observation sequence, we have simulated the survey based on the weather history, sky noise, and depth of the PS1 SN survey (Scolnic et al. 2014b) at various exposure times. We then fit the simulated light curves and recovered light-curve parameters. We find that at our lowest exposure time of 15 s, colour errors are typically 0.03–0.04 mag and distance errors are typically 0.10–0.12 mag, in line with our goals.

We have examined this strategy with our survey data (see Section 3). For each SN observed, we can compare the final distance error to the number of epochs observed, which we display in Fig. 1. We note that these are the number of observed epochs, not the number of epochs used when fitting the light curves, where particularly early or late data are not included. We find that the typical distance uncertainty is <0.10 mag for SNe with an average of ≥3.6 epochs per band. We also find that if an SN is observed prior to 7 d after peak brightness generally produces small distance uncertainties (Fig. 2). For the Foundation Supernova sample, we find that both criteria are necessary to have confidence in our distance moduli.

2.4.3 *Data quality*

We limit our observations to have an airmass below 2, extinction due to clouds of <0.5 mag, and seeing with FWHM <1.8 arcsec. We place each SN at a random place on the focal plane, restricted to areas known to produce high-quality images (e.g. >0.°4 from the centre of the focal plane; Rest et al. 2014) and away from

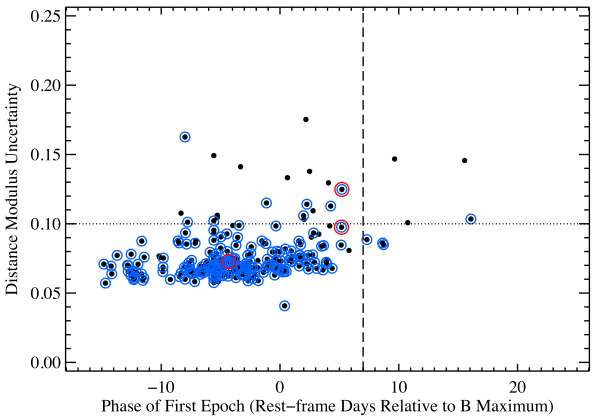

Figure 2. Same as Fig. 1, except as a function of the phase of the first epoch for the Foundation sample. Here, the red circles indicate SNe that pass all criteria *except* they have too few epochs for inclusion. The vertical dashed line represents the first-epoch phase necessary for inclusion in the cosmology sample. Objects with a first epoch at a phase of $<+7$ d have typical distance uncertainties of ≤ 0.10 mag.

known detector defects and chip gaps. For each SN, the location does not vary for $>0\overset{\circ}{.}05$ for the entire light curve. As a result, we reduce potential systematic biases related to a particular detector or position in the focal plane, which is a 3-mmag bias across the entire focal plane (Scolnic et al. 2014b).

The morning after an observation, we check the SN location to make sure that the nearby area has not been masked, that there are no artefacts near the SN, and that the SN is sufficiently far from chip gaps. If there are any issues with the observation, we immediately request a new observation. We have requested repeat observations because of problems in an image for only 1.1 per cent of our observations.

For the nights where we requested observations, 39 per cent were weathered out. In these cases, we immediately request a new observation. Based on our current data set, we have found that our median cadence near peak is 6d, close to our desired value of 5 d. The reason for this difference is primarily caused by periods of extended bad weather. Our median seeing is 1.28, 1.16, 1.05, and 1.02arcsec in $griz_{\rm P1}$, respectively.

Observations typically saturate at 12.5 mag for 15-s exposures. This is much brighter than any of our SN observations. Furthermore, we expect any non-linearities due to the brighter-fatter effect (Antilogus et al. 2014) to be <2 mmag at $m > 13$ mag. The typical number of stars per CCD that overlap with calibrated stars from the 3π survey is >500 stars. Typical uncertainties in our nightly photometric zero-points are 3 mmag.

2.4.4 *Sample size*

For any cosmological analysis using the Foundation sample, the statistical uncertainties will depend, in part, on the number of SNe in the Foundation sample. Since cosmological measurements depend on comparing the *relative* distances to SNe, a large sample of low-z SNe is critical for precise measurement of cosmological parameters. There are currently ∼1000 published high-quality high-z SNe Ia (Scolnic et al. 2017), about five times the size of the current low-z sample. As such, a single low-z SN Ia currently has more statistical weight than a single high-z SN Ia. Moreover, observations at longer rest-frame wavelengths, where the SNe suffer less dust extinction and have lower intrinsic scatter (e.g. Krisciunas, Phillips & Suntzeff 2004; Wood-Vasey et al. 2007; Folatelli et al. 2010; Mandel, Narayan & Kirshner 2011; Stritzinger et al. 2011; Barone-Nugent et al. 2012; Friedman et al. 2015), are easier to obtain at low z. Therefore, observing low-z SNe is a relatively economical approach to improving the statistical uncertainties on cosmological parameters.

However, gains will steadily decrease as the statistical uncertainty approaches the systematic uncertainty. If we can produce a low-z SN Ia sample that is the same size as the current sample, but with smaller systematic uncertainties, that is a clear improvement. The Foundation sample will have calibration uncertainties similar to that of the PS1 high-z sample, which are one-third that of the current low-z sample (Scolnic et al. 2015). As the current low-z sample contains ∼200 SNe Ia, a first goal for the Foundation sample is to match that number.

To demonstrate the power of the reduced systematic uncertainties associated with the Foundation Supernova Survey, we performed multiple simulations using the SNANA simulation package (Kessler et al. 2009). The simulations match all key characteristics of the surveys including cadence, S/N, and detection/spectroscopic selection functions. As has been done in past cosmology analyses (Betoule et al. 2014; Scolnic et al. 2014b, 2017), the selection functions have been empirically determined such that each simulation produces the observed redshift distribution as well as the observed light-curve shape/colour distributions as a function of redshift. In the future, we will directly include detection efficiencies of the ASAS-SN and PSST surveys to better constrain the overall Foundation Supernova Survey selection function. Our accurate simulations will allow us to correct for any distance biases with redshift, colour and stretch (Scolnic & Kessler 2016).

As a baseline, we simulated the current SN Ia sample, including the current low-z sample (Rest et al. 2014, but set to have exactly 200 SNe Ia for simplicity), the Joint Light-curve Analysis (JLA) high-z sample (Betoule et al. 2014), and the PS1 high-z sample (Rest et al. 2014). SNANA generates light curves as would be observed by each survey that contributes to the final sample.

Once the Foundation Supernova Survey data are incorporated in SN spectral models, the reduced calibration uncertainties will improve the SN spectral model uncertainties by ∼25 per cent (Scolnic et al., in preparation), which is roughly the fraction of low-z SNe in the current training set. For all simulations, we include the same level of systematic uncertainties from the absolute calibration of the *HST* Calspec standards and MW extinction. No other systematic uncertainties are included; for instance those related to selection biases are excluded (although we expect to improve such uncertainties with the Foundation Supernova Survey in the future).

Cosmological constraints are determined from use of the Markov Chain Monte Carlo technique implemented with the COSMOMC code (Lewis, Challinor & Lasenby 2000). The cosmological parameters are all given non-informative priors. For all measurements in this paper, we assume a flat universe and marginalize over H_0 and Ω_M.

When we combine the simulated current low-z SN and JLA samples with CMB (Planck Collaboration XIII 2016) and BAO (Anderson et al. 2014) data, and assume a constant dark energy equation of state, we find the uncertainty for w to be $\mathrm{d}w = 0.053$, comparable to that found by Betoule et al. (2014), $\mathrm{d}w = 0.055$.[3] We

[3] While the simulated results produce slightly better results (by 8 per cent in precision) than the real data, this is likely because of the updated CMB constraints used for the simulations.

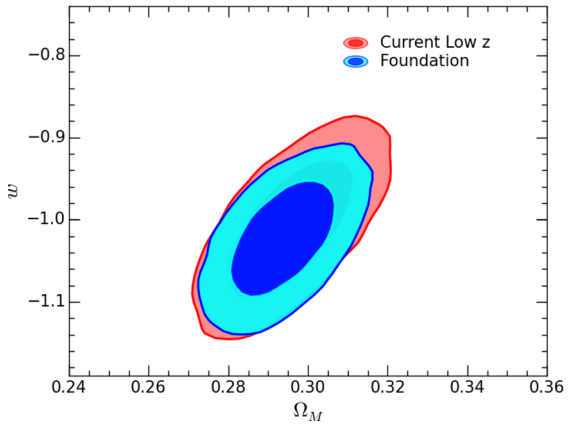

Figure 3. 1σ and 2σ confidence contours in the w–$\Omega_{\rm m}$ plane for simulated SN data. The pink/red and teal/blue contours represent the projected constraints from current CMB (Planck Collaboration XIII 2016), the simulated JLA high-z SN compilation (Betoule et al. 2014), and either a simulation that roughly matches the current low-z SN Ia sample (but with exactly 200 SNe Ia) or a simulated Foundation Supernova sample (with exactly 200 SNe Ia), respectively. Including systematic uncertainties, the marginalized uncertainty for w improves from 0.053 to 0.046, a 35 per cent improvement in precision, when replacing the current low-z sample with an equal-sized Foundation sample.

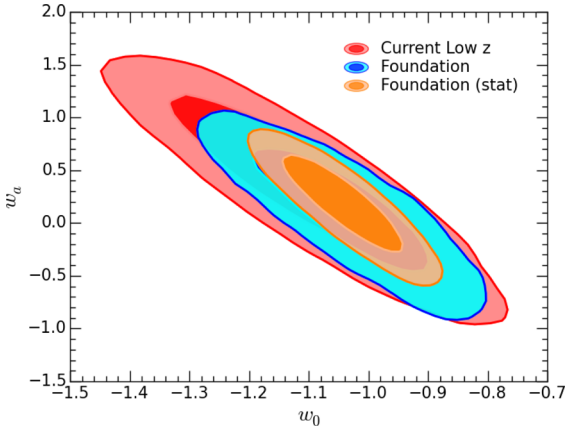

Figure 4. 1σ and 2σ confidence contours in the w_0–w_a plane for simulated SN data. The pink/red and teal/blue contours represent the projected constraints from current CMB (Planck Collaboration XIII 2016), a simulated PS1/DES photometric sample of 3500 high-z SNe Ia, and either the current low-z SN Ia sample or 200 Foundation SNe Ia, respectively. The tangerine/orange contours represent what we would expect in the absence of any systematic uncertainties. The dark energy FoM improves from 30 to 52, a 72 per cent improvement, when replacing the current low-z sample with an equal-sized Foundation sample.

display the w–$\Omega_{\rm m}$ confidence contours derived from these simulated data in Fig. 3.

We also simulated a sample of 200 Foundation SNe. The combination of the simulated Foundation sample, JLA high-z sample, CMB data, and assuming a constant equation of state, results in a uncertainty for w of $\mathrm{d}w = 0.046$ (w–$\Omega_{\rm m}$ confidence contours are shown in Fig. 3). That is, simply replacing the current low-z SN Ia sample with the same number of SNe from the Foundation sample is predicted to result in a 35 per cent improvement in precision for our measurement of w.

In the next few years, significantly larger samples of high-z SNe ($\sim$ 5000 SNe Ia) from DES (Bernstein et al. 2012) and PS1 (Rest et al. 2014) will be available. With these larger samples, we will be able to place relatively tight constraints on evolving dark energy. We simulated 3500 high-z SNe and set the calibration systematic uncertainty to be the same as PS1. Combining these data with the simulated, current low-z, and Foundation Supernova Survey samples (and now allowing for an evolving equation of state), we find dark energy FoMs of 30 and 52, respectively (Fig. 4). That is, replacing the current low-z sample with an equally sized Foundation Supernova sample will improve the dark energy FoM by 72 per cent.

As shown from our simulations, a Foundation sample of $\sim$200 SNe Ia is well motivated. However, larger sample sizes, up to at least 800 SNe, will also significantly improve cosmological inference *if* potential calibration systematics are appropriately reduced.

In their final report, the *WFIRST* Science Definition Team (Spergel et al. 2015) determined that a low-z sample of 800 SNe Ia is *required* to reach their science goals. While this is further confirmation of the importance of a large high-fidelity low-z SN Ia sample, it also presents an independently derived number for a final sample size. While 200 or 400 Foundation SNe Ia would potentially be a significant fraction of the final *WFIRST* low-z required sample, it is possible for the Foundation sample to be the entire *WFIRST* low-z sample within 4 yr of operations.

Detailed simulations of the *WFIRST* survey are underway (Hounsell et al. 2017), and we will revisit the necessary low-z sample size in the future.

3 OBSERVATIONS AND DATA REDUCTION

As of May 2017, we have observed a total of 342 SNe with PS1. Of these, 169 were snapshot observations that were not continued. We have followed 225 SNe Ia, whose light curves are presented below. Most observations are a series of 15-s $griz_{\rm P1}$ exposures. Our earliest observations were obtained in twilight as a pilot programme and had 100-s exposures.

We reduce the Foundation PS1 data with the same custom-built pipeline as for the PS1 MDF survey data. The basic data processing is performed by the PS1 IPP (Magnier 2006; Magnier et al. 2013; Waters et al. 2016). Downstream processing is performed with the `photpipe` pipeline that members of our team developed for the SuperMACHO and ESSENCE surveys (Rest et al. 2005; Miknaitis et al. 2007; Rest et al. 2014; Scolnic et al. 2014b; Narayan et al. 2016a).

The PS1 IPP system performs flat-fielding on each individual image, using white-light flat-field images of a dome screen, in combination with an illumination correction obtained by rastering sources across the FOV. After determining an initial astrometric solution (Magnier et al. 2008, 2016), the flat-fielded images are then warped on to the tangent plane of the sky, using a flux-conserving algorithm. We present an example SN image in Fig. 5.

High-quality images of a given SN location obtained during the 3π survey are stacked, allowing for the removal of defects such as cosmic rays and satellite streaks. Since the 3π survey finished in 2014, these images are free of SN flux for the Foundation sample. The stacked images typically go much deeper than the Foundation Supernova Survey data, with typical limiting magnitudes of 23.0, 22.9, 22.9, and 22.2 in $griz_{\rm P1}$, respectively (Chambers et al. 2016).

Single-epoch Foundation Supernova Survey images are then processed through a frame-subtraction analysis using `photpipe`. This robust and well-tested system first determines the appropriate

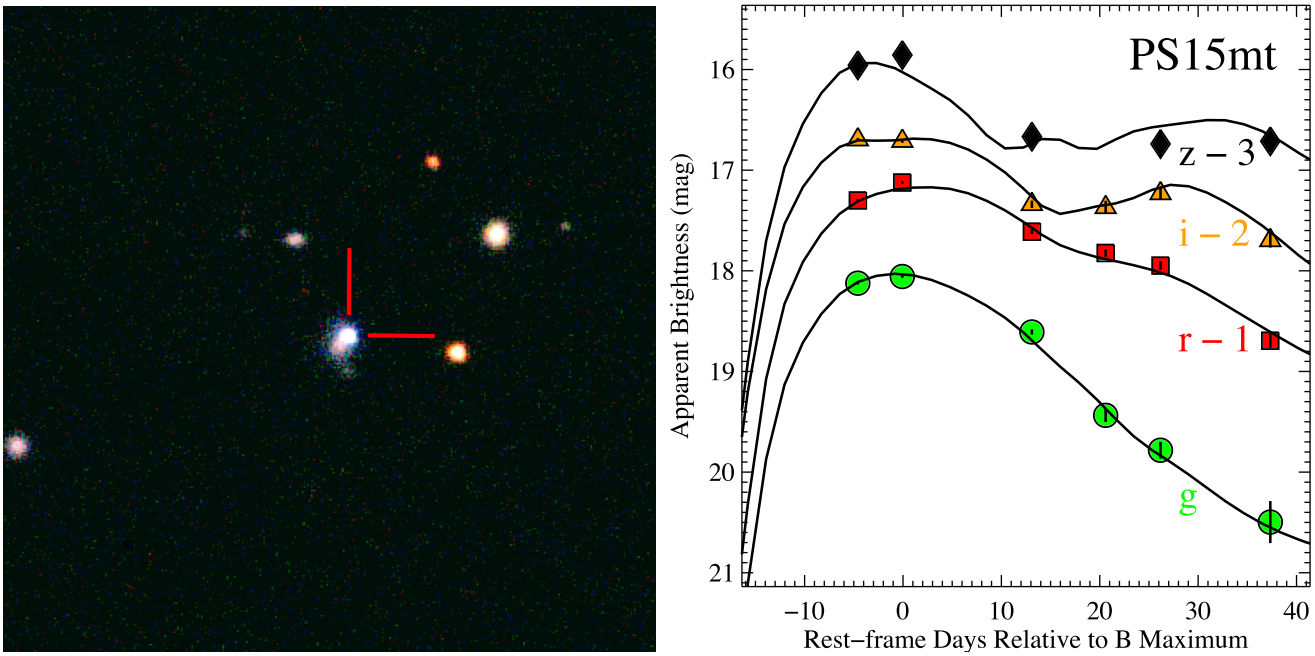

Figure 5. (*Left*) 90 arcsec × 90 arcsec PS1 *gri* (corresponding to BGR channels) image of PS15mt. The image is oriented with north up and east left. The SN is marked by the red tick marks. (*Right*) Multicolour light curves for PS15mt. $griz_{P1}$ photometry are plotted as green circles, red squares, orange triangles, and black diamonds, respectively. Photometric uncertainties are plotted, but are typically smaller than the points. The black lines are SALT2 model fits to the light curves. The z-band fits are only illustrative; those data are not currently used to measure distances.

spatially varying convolution kernel using HOTPANTS (Becker 2015); this kernel is necessary to match the template image to the survey image. After the convolution is performed, the template image is subtracted from the survey image. We then detect significant flux excursions in the difference images using DOPHOT (Schechter, Mateo & Saha 1993).

For each SN, we calculate the weighted average position using detections from all bands. Because almost all of the SNe are measured with high SNR (>50) near peak and each have ∼5 exposures, the typical uncertainty of the SN location is <0.1 pixels. We perform 'forced' photometry for this position for all epochs for a particular SN. This is the same method as used for Rest et al. (2014), with the only difference being that we currently use DOPHOT instead of DAOPHOT. The median difference between forced and unforced photometry is ∼1.5 mmag for the brighter detections, and is slightly larger for low-S/N detections. The latter difference is the result of an Eddington bias in the flux of measurements detected without forced photometry.

Zero-points are determined from comparing measurements of stars in the survey image to those in the 3π catalogue. The median zero-point uncertainty is ∼3 mmag per band. We present example light curves for a single SN in Fig. 5. Eventually, we plan to re-reduce the photometry with a process similar to that of DAOPHOT (Stetson 1987) with forced photometry on all subtracted images. This process has been done for the high-z PS1 data (Rest et al. 2014), including modifications to minimize systematic uncertainties in the photometry.

For the Foundation Supernova Survey, we must carefully measure the system throughput as the filters may have changed since the initial PS1 calibration was performed. During the 1.5 yr of the initial PS1 survey, no changes were detected to a limit of 3 mmag (Rest et al. 2014). This analysis will be extended for the entire 4.5-yr PS1 survey. However, for the Foundation Supernova Survey, which will observe well past the initial PS1 survey, we plan to continue to monitor the system throughput. The majority of PS1 observations are not for the Foundation Supernova Survey, but every $griz_{P1}$ image that PS1 observes provides a direct comparison for hundreds of stars. We will use these data, along with specific calibration frames, to track the system throughput for the duration of the Foundation Supernova Survey.

Detailed information about the SNe in our sample is presented in Table 1. We present photometry of our current sample, corresponding to the first data release (DR1) of the Foundation Supernova Survey, in Table 2 and display their light curves in Fig. 6.

4 ADDITIONAL DATA

If the Foundation sample is to become the benchmark low-z SN Ia sample, it must include data beyond the PS1 SN photometry. In particular, SN spectroscopy, SN NIR photometry, and host-galaxy data are all potentially important.

SN spectroscopy is critical for proper SN classification. While public classifications are generally reliable, some are incorrect. We therefore attempt to obtain our own spectrum of every Foundation SN to verify its classification. For some SNe, these data will also provide the first spectroscopic redshifts of their host galaxies. For $z < 0.08$, redshift uncertainties can propagate to a relatively large distance uncertainty. For instance, at $z = 0.015$, 0.033, and 0.08 (our nominal minimum, median, and maximum redshifts for the Foundation sample), a redshift uncertainty of 0.01 propagates to a distance modulus uncertainty of 2.40, 1.10, and 0.15 mag, respectively.

SN spectral data also have the ability to significantly improve SN distance estimates (e.g. Bailey et al. 2009; Blondin, Mandel & Kirshner 2011; Chotard et al. 2011; Foley & Kasen 2011; Foley, Sanders & Kirshner 2011; Foley 2012; Silverman et al. 2012; Mandel, Foley & Kirshner 2014). Specifically, the intrinsic colour

Table 1. Foundation supernova sample data.

IAU name	Discovery name	Alternative names	Galaxy	Discovery ref.	Classification ref.	Type
2015I	PSN J07174570+2320406		NGC 2357	CBET 4106	ATEL 7476	
2015M	PSN J13003230+2758411	CSS150521:130032+275841	COMAi J130032.301+275841.02	CBET 4123	ATEL 7528	06gz
		KISS15n		ATEL 7532	ATEL 7529	
		PS15apc			ATEL 7532	
2015ar	PSN J01072038+3223598	CSS151130:010720+322359	NGC 383	CBET 4193	ATEL 8291	
2015az	PSN J03094251+4058293	PS15dqn	IC 290	CBET 4208	ATEL 8348	
2016E	PS16n		2MASX J05034387+0324429	ATEL 8524	ATEL 8524	
2016F	ASASSN-16ad	CSS160204:013932+334936	KUG 0136+335	ATEL 8521	ATEL 8532	
2016H	PS16fa		CGCG 036-091	ATEL 8534	ATEL 8534	
2016J	PS15dpl		Anonymous	GCN 18786	GCN 18811	
	ASASSN-16ah			ATEL 8539	ATEL 8539	
2016K	ASASSN-16aj	PS16rs	NGC 1562	ATEL 8542	ATEL 8550	
2016W	PSN J02303969+4214089		NGC 946	TNS	ATEL 8580	
2016ac	ASASSN-16av		NGC 3926 NED02	ATEL 8569	ATEL 8636	
2016ah	PS16el		2MASX J10511252+1921474	ATEL 8524	ATEL 8524	
2016ai	PS16ez		SDSS J092426.62+051018.1	ATEL 8524	ATEL 8524	91T
2016ys	ASASSN-16ay		UGC 3738	ATEL 8609	ATEL 8613	
2016zd	ASASSN-16bc	PS16aqd	2MASX J12052488−2123572	ATEL 8628	ATEL 8634	
2016acs	PS16aer		CGCG 95-67	ATEL 8663	ATEL 8663	
2016aew	ASASSN-16bq		IC 986	ATEL 8685	ATEL 8694	
2016aex	ASASSN-16br		2MASX J15453055−1309057	ATEL 8685	ATEL 8694	91T
2016afb	CSS160129:074030+105600	PS16acs	Anonymous	ATEL 8613	ATEL 8613	
2016afk	PS16agp		2MASXi J1022298+150547	ATEL 8702	ATEL 8702	
2016ajf			NGC 1278	TNS	ATEL 8713	91bg
2016ajl			2MASX J04422451−2143312	ATEL 8716	ATEL 8719	
2016alt	PS16amf		GALEXASC J063701.16+441611.9	TNS	TNS	06gz
2016aqa	LSQ16sf		LCRS B112120.0−051639	ATEL 8739	ATEL 8739	91T
2016aqb	LSQ16te		2MASXi J1121579−135849	ATEL 8739	ATEL 8739	91T
2016aqs	Gaia16agf	PS16aro	Anonymous	ATEL 8754	ATEL 8754	
2016aqt		CSS160307:134551+264747	SDSS J134550.90+264747.4	TNS	ATEL 8774	91T
		PS16asv				
2016aqz	ASASSN-16ch	PS16brh	CGCG 101-008	ATEL 8763	ATEL 8771	
2016arc	ASASSN-16ci		NGC 1272	ATEL 8765	ATEL 8765	91bg
2016asf	ASASSN-16cs	ATLAS16aep	KUG 0647+311	ATEL 8784	ATEL 8788	
2016aud	ASASSN-16ct		SDSS J151354.30+044525.7	ATEL 8796	ATEL 8798	91T
2016axb	PS16axi		2MASX J10480747+0010017	TNS	ATEL 8822	
2016axw	MASTER OT J142718.40-014031.0	PS16ayd	2MASX J14271887−0140428	ATEL 8791	ATEL 8823	
2016ayf	ASASSN-16cy		CGCG 295-010	ATEL 8801	ATEL 8830	91T
2016ayg	PTSS-16hs	Gaia16ahw	SDSS J073017.25+250153.5	TNS	ATEL 8824	
2016baq	SNhunt313	ASASSN-16db	UGC 06198	TNS	ATEL 8833	
		2016bcy		ATEL 8813		
2016bew	LSQ16acz	PS16bby	2MASX J14201699−2211186	TNS	ATEL 8829	
2016bey	ATLAS16ahj		2MASX J11374023+5704420	TNS	ATEL 8844	
2016bfc	ATLAS16agv		Anonymous	TNS	ATEL 8844	
2016bkw	Gaia16acv	PS16aqu	SDSS J115949.80+544807.1	TNS	ATEL 8683	
2016blc	ASASSN-16dn	CSS160404:104849-201550	GALEXASC J104848.62−201544.1	ATEL 8885	ATEL 8896	
		PS16brg				
2016blg	PTSS-16cfd	MASTER OT J132713.97-021611.8	SDSS J132713.81−021615.2	TNS	ATEL 8906	
		MLS160401:132714-021613				
2016blh	PTSS-16cfg	PS16boq	CGCG 018-062	TNS	ATEL 8899	
2016blj	ASASSN-16dw	PS16cce	2MASX J13300119−2758297	ATEL 8897	ATEL 8902	
2016blm	LSQ16ahs	PS16bom	Anonymous	TNS	ATEL 8902	
2016bln	iPTF16abc	MASTER OT J133445.47+135113.8	NGC 5221	ATEL 8907	ATEL 8909	91T
		PS16brj				
		CSS160417:133446+135114				
2016bmc	ASASSN-16ej		UGC 11409	ATEL 8839	ATEL 8955	
2016bmh	ASASSN-16em		GALEXASC J133213.24+844042.7	ATEL 8953	ATEL 8953	
2016bpb	PS16bnz		UGC 05586 NED02	TNS	ATEL 8918	
2016cby	ASASSN-16et	iPTF16aiw	2MASX J10200192+5627397	ATEL 9005	ATEL 9026	
2016ccj	ASASSN-16ex	CSS160513:171024+262348	SDSS J171023.63+262350.3	ATEL 9020	ATEL 9023	06gz
					ATEL 9024	
2016cck	PTSS-16efw		2MASX J17353788+0848387	TNS	ATEL 9023	
					ATEL 9025	

Table 1 – *continued*

IAU name	Discovery name	Alternative names	Galaxy	Discovery ref.	Classification ref.	Type
2016ccz	iPTF16auf	PS16cpd Gaia16aqm	MRK 685	ATEL 9049	ATEL 9049	
2016cob	ASASSN-16fo		2MASX J13323577−0516218	ATEL 9081	ATEL 9099	91T
2016coj	KAIT-16X	AT2016cop	NGC 4125	ATEL 9095	ATEL 9095	
2016cor		PS16crs	SDSS J154431.47+161814.0	TNS	TNS	
2016cpy	ASASSN-16fs	SNhunt317	UGC 9523	ATEL 9114	ATEL 9129	
2016cuv			GALEXASC J161914.56+402512.5	TNS	TNS	
2016cvn	ATLAS16bdg		NGC 4708	ATEL 9151	ATEL 9165	
2016cvv	PTSS-16ijc	PS16cyd	CGCG 280-24	TNS	ATEL 9171	
2016cvw	PTSS-16ipw		MCG +2-58-8	TNS	ATEL 9173	
2016cxb	MASTER OT J211223.35+144645.1	PS16cvc	GALEXASC J211223.05+144644.9	ATEL 9174	ATEL 9182	
2016cyt		PS16dst	NGC 7033	TNS	ATEL 9210	
2016czc	ASASSN-16hc		2MASX J13590394+3308172	ATEL 9223	ATEL 9237	91T
2016dxe	Gaia16aki		SDSS J155910.36+143829.4	TNS	ATEL 8934	
2016dxv	Gaia16alq	PS16ccn	Anonymous	TNS	ATEL 8991	
2016eee	CSS160428:132307+523857	Gaia16ash	SDSS J132307.25+523858.1	TNS	ATEL 9019	
2016eja	ASASSN-16hr	Gaia16azu	2MASX J22253147+3859010	ATEL 9270	ATEL 9273	
2016eky	PS16dnp	CSS160904:225940+020859 MASTER OT J225939.54+020859.6	2MASX J22593744+0209095	TNS ATEL 9297	ATEL 9302	
2016enx	ATLAS16bwu		GALEXASC J011422.73−130915.9	TNS	ATEL 9377	91T
2016eoa		PS16env Gaia16bay	NGC 83	TNS	ATEL 9335	
2016eqb	ASASSN-16hz		2MASX J23154564−0120135	ATEL 9332	ATEL 9333	
2016esh	ASASSN-16ie		2MASXi J1604144+164124	ATEL 9341	ATEL 9345	
2016euj	ASASSN-16ip		ESO 479-G7	ATEL 9353	ATEL 9368 ATEL 9372	
2016ews	Gaia16bby		IC 4526	TNS	ATEL 9381	91T?
2016fbk			UGC 1212	TNS	ATEL 9384	
2016fbo	Gaia16bba	CSS160829:010136+170605 MLS160905:010136+170605	GALEXASC J010135.75+170604.9	TNS	ATEL 9421	
2016fff	ASASSN-16jf	PS16eqt	UGCA 430	ATEL 9398	ATEL 9406	
2016ffh	ATLAS16cpu	Gaia16bcm	CGCG 249-11	ATEL 9400	ATEL 9403	
2016gfr			2MASX J18193566+2347137	TNS	TNS	
2016ghq			UGC 11199	TNS	ATEL 9532	
2016gkt	PS16ejh		ESO 472- G 013	ATEL 9531	ATEL 9549	
2016glp	PS16ejp		GALEXASC J233613.95+234146.7	TNS	ATEL 9542	
2016glz	CSS160922:000554+082548	PS16eoc iPTF16glz	GALEXASC J000556.57+082613.6	TNS	TNS	
2016gmb	PTSS-16oqc		GALEXASC J003445.02-060936.8	TNS	ATEL 9542	
2016gmg	PTSS-16opy	Gaia16bky	2MASX J21234100+3307075	TNS	ATEL 9569	
2016gou	ATLAS16cxr		Anonymous	TNS	ATEL 9549	
2016grz			SDSS J015533.01+334921.3	TNS	ATEL 9583	
2016gsn	ASASSN-16la	PS16esq	2MASXi J0229172+180515	ATEL 9571	ATEL 9581	
2016gsu	PTSS-16pur		SDSS J010824.54+210906.3	TNS	ATEL 9607	
2016gye	ASASSN-16lg		ARK 530	ATEL 9601	ATEL 9610	
2016hgw	ATLAS16dpb	iPTF16hgw	CGCG 415-40	ATEL 9685	ATEL 9696	
2016hhv	ATLAS16drn		2MASX J23354784+2042265	TNS	ATEL 9706	
2016hjk	PS16eqv		2MASX J02314347-2500088	TNS	ATEL 9682	91T
2016hli	ATLAS16dod		MCG +08-07-008	ATEL 9685	ATEL 9695	
2016hns	ATLAS16dpv		KUG 2137+241	ATEL 9685	ATEL 9696	
2016hot	CSS161013:015319+171853	PS16etp ATLAS16dna	Anonymous	TNS	ATEL 9695	91T
2016hpx	Gaia16bwt	ATLAS16dqh PS17aji	2MASXi J0603164-265353	TNS	ATEL 9704	
2016hqf	PS16evk		2MASX J22332338-0121266	TNS	ATEL 9711	91T
2016htm	ATLAS16dsh	Gaia16bvq PS16fci	2MASX J02320134-2639576	TNS	ATEL 9711	
2016htn	ATLAS16dsj	PS16fch Gaia16bxx	2MASX J02112819-1630409	TNS	ATEL 9711	
2016ick	PS16fbb	Gaia16bvg	GALEXASC J000703.01-204149.5	TNS	ATEL 9793	
2016idy	MASTER OT J013415.01-174843.9	PS16fbm	GALEXASC J013415.00-174836.1	ATEL 9540	ATEL 9597	
2016ixf	Gaia16cdf	PS17bll	SDSS J103944.53+150204.7	TNS	ATEL 9889	
2016iyv	ASASSN-16oz	Gaia16cgf PS17bqr	GALEXASC J090013.19-133803.5	ATEL 9887	ATEL 9889	91T

Table 1 – *continued*

IAU name	Discovery name	Alternative names	Galaxy	Discovery ref.	Classification ref.	Type
2016jem	ATLAS16eej		GALEXASC J235216.94−224520.3	TNS	ATEL 9930	
2017dz	iPTF17dz	PS17amw	SDSS J082425.68+245951.5	GCN 20398	GCN 20408	
2017hm	ASASSN-17aj	PS17bhh	MCG -02-30-003	ATEL 9952	ATEL 9968	
2017hn		PS17bpa	UGC 8204	TNS	ATEL 9959	
2017jl	ATLAS17air		2MASX J00573150+3011098	TNS	ATEL 9990	91T?
2017lc	Gaia17aea		Anonymous	TNS	ATEL 9990	00cx?; 91bg?
2017lm	ATLAS17aix	Gaia17akm	2MASX J03013238−1501028	TNS	ATEL 9981	
2017ln	ASASSN-17at	PS17bhi	2MASX J11383367+2523532	ATEL 9989	ATEL 9980	
2017lv	ATLAS17ajn		ESO 440-G1	TNS	ATEL 10012	
2017me	ATLAS17ajs	PS17bhg	KUG 1125+276	TNS	ATEL 10012	
2017mf		Gaia17ano	NGC 5541	TNS	ATEL 9986	
2017ms	PTSS-17dfc	PS17cfh	SDSS J102641.99+364053.2	TNS	ATEL 9991	
		Gaia17axi			ATEL 9992	
2017mu	PTSS-17dgm	PS17qr	GALEXASC J093036.72+212437.4	TNS	ATEL 10018	06gz
2017nk	ASASSN-17bd		2MASX J15591858+1336487	ATEL 10000	ATEL 10014	91T
2017ns	ATLAS17alb	PS17agl	2MASX J02491020+1436036	TNS	ATEL 9996	
		Gaia17akz				
2017nw	ATLAS17ali	PS17atr	SDSS J111612.52+024828.9	TNS	ATEL 10010	
2017oz	ATLAS17amc		SDSS J140641.53+301906.5	TNS	ATEL 10032	
2017po	ASASSN-17bh	Gaia17ait	UGC 10166[a]	ATEL 10013	ATEL 10032	
		CSS170130:160352+395924				
2017wb	ASASSN-17bo	PS17awj	2MASX J11011991+7039548	ATEL 10022	ATEL 10026	
		Gaia17air				
2017ya	ATLAS17arb		SDSS J001644.50+152030.6	TNS	ATEL 10032	
2017yh	ASASSN-17bs	Gaia17ahm	IC 1269	ATEL 10031	ATEL 10041	
2017yk	ATLAS17asj	PS17bqx	2MASX J09443215−1218233	TNS	ATEL 10032	
2017zd	ATLAS17auc		2MASX J13324217−2148034	TNS	ATEL 10053	
2017aaa	PS17akj	Gaia17alw	LCRS B134713.8−024957	TNS	ATEL 10056	
2017adj	ATLAS17axb	Gaia17amq	GALEXASC J134322.97−195637.5	TNS	ATEL 10056	
		PS17bws				
2017awz	ATLAS17bas		SDSS J110735.45+225104.1	TNS	ATEL 10094	91T
2017azk	PS17bii		2MASX J11253836+0720042	TNS	ATEL 10124	
2017cfb	ATLAS17cof	PS17bwt	CGCG 073-094	TNS	ATEL 10178	
		CSS170417:135407+092446				
		Gaia17blj				
2017cfc	ATLAS17cog	PS17cfr	UGC 8783	TNS	ATEL 10212	
2017cfd	kait-17I	Gaia17avm	IC 511	TNS	ATEL 10182	
		PS17ceu				
2017cgr	MASTER OT J083256.92−035128.1	PS17bup	2MASX J08325728−0351295	ATEL 10074	ATEL 10093	
		Gaia17atq				
2017cii	ASASSN-17du	Gaia17baa	SDSS J163319.94+234356.4	ATEL 10200	ATEL 10212	
		PS17dbv				
		ATLAS17byo				
2017ciy	ATLAS17daf	MLS170408:170407+250310	2MASX J17040672+2503184	TNS	ATEL 10212	
		Gaia17azx				
		PS17cyr				
2017cju	ASASSN-17eb	PS17dbp	2MASX J15383353+1320423	ATEL 10206	ATEL 10207	
2017cjv	ATLAS17dda	PS17cci	LCRS B100813.8-033156	TNS	ATEL 10212	
2017ckd	PTSS-17niq	PS17bww	2MASX J14201616+1520386	TNS	ATEL 10225	
2017ckx	ASASSN-17ee		UGC 4030 NED01	ATEL 10232	ATEL 10232	
2017coa			SDSS J084955.19+560554.6	TNS	ATEL 10235	
2017cpu	ASASSN-17ej	PS17ckr	2MASX J14075270+0938281	ATEL 10241	TNS	
	ASASSN-15bc		LEDA 170061	ATEL 6943	ATEL 6949	91T
					ATEL 6956	
	ASASSN-15bm		GALEXASC J150551.56−053737.2	ATEL 6983	ATEL 6988	
	ASASSN-15fa	Gaia15adb	NGC 6319	ATEL 7245	ATEL 7253	91T
	ASASSN-15fs	Gaia15afh	CGCG 229-10	ATEL 7296	ATEL 7306	
		PS15aij				
	ASASSN-15ga		NGC 4866	ATEL 7317	ATEL 7333	91bg
	ASASSN-15go		2MASX J06113048−1629085	ATEL 7349	ATEL 7368	
					ATEL 7375	
	ASASSN-15hg		CGCG 63-98	ATEL 7413	ATEL 7420	
					ATEL 7421	

Table 1 – *continued*

IAU name	Discovery name	Alternative names	Galaxy	Discovery ref.	Classification ref.	Type
	ASASSN-15hy	PS15aou	Anonymous	ATEL 7450	ATEL 7452	06gz
	ASASSN-15il		2MASX J15570808−1240252	ATEL 7491	ATEL 7497	
	ASASSN-15jl	PS15aol	SDSS J152241.16+505836.0	ATEL 7527	ATEL 7535	
	ASASSN-15jt		2MASX J13080914+2749354	ATEL 7551	ATEL 7558	
	ASASSN-15kx		MCG +6-49-1	ATEL 7621	ATEL 7623	
	ASASSN-15la	PS15bdj	NGC 5517	ATEL 7626	ATEL 7627	
	ASASSN-15lg		CGCG 44-42	ATEL 7635	ATEL 7640 ATEL 7644	
	ASASSN-15lu		SDSS J132112.88+401556.7	ATEL 7698	ATEL 7707	91T
	ASASSN-15mf		UGC 9108 NED02	ATEL 7775	ATEL 7781	
	ASASSN-15mg		2MASX J15322270+4150586	ATEL 7780	ATEL 7787	
	ASASSN-15mi		MRK 283a	ATEL 7790	ATEL 7796	91T
	ASASSN-15np		2MASX J15060265+0733415	ATEL 7878	ATEL 7888	
	ASASSN-15nq		2MFGC 13779	ATEL 7880	ATEL 7885 ATEL 7888	
	ASASSN-15nr		CGCG 82-31	ATEL 7881	ATEL 7882	91T
	ASASSN-15od	DES15X3iv	MCG -1-7-4	ATEL 7907	ATEL 7913 ATEL 8167	
	ASASSN-15oh		MCG +6-49-27	ATEL 7911	ATEL 7924	
	ASASSN-15pm	CSS150913:013836-044047	2MASX J01383676−0440581	ATEL 8041	ATEL 8072	
	ASASSN-15pn		SDSS J040326.23−052930.6	ATEL 8041	ATEL 8072 ATEL 8073	
	ASASSN-15pr		2MASX J23063962−1234238	ATEL 8051	ATEL 8072 ATEL 8073	
	ASASSN-15py		SDSS J080519.59+225751.1	ATEL 8098	ATEL 8105	
	ASASSN-15rw	CSS151031:021558+121414 MLS151211:021558+121414 PS15coh	GALEXASC J021558.44+121415.2	ATEL 8212	ATEL 8239 ATEL 8249	
	ASASSN-15sb		2MFGC 04848	ATEL 8217	ATEL 8217	
	ASASSN-15sf	LSQ15bjb PS15cog	GALEXASC J001127.51−062549.8	ATEL 8226	ATEL 8230	
	ASASSN-15so		NGC 3583	ATEL 8256	ATEL 8259 ATEL 8261	
	ASASSN-15ss		MCG -2-16-4	ATEL 8273	ATEL 8279	
	ASASSN-15tg	Gaia16afu	GALEXASC J002041.66+251341.1	ATEL 8347	ATEL 8350	91T
	ASASSN-15ti		2MASX J03051061+3754003	ATEL 8351	ATEL 8356	
	ASASSN-15tz		UGC 2164	ATEL 8404	ATEL 8410	
	ASASSN-15uu		MCG +3-5-13	ATEL 8480	ATEL 8495	
	ASASSN-15uv	PS15dqu	2MASX J08270817+2748382	ATEL 8488	ATEL 8493	
	ASASSN-15uw		2MASX J02353437−0603496	ATEL 8490	ATEL 8506	
	CSS151120:044526-190158		Anonymous	ATEL 8320	ATEL 8320	91T
	iPTF17fs		Anonymous	GCN 20401	GCN 20409	
	MASTER OT J151647.17+283742.8	CSS160712:151647+283743	2MASX J15164763+2837061	ATEL 9204	ATEL 9243	
	MASTER OT J222232.87-185224.3	PSN J22223287−1852243	IC 5210	ATEL 7632	ATEL 7640	91bg
	PS15mt		SDSS J095444.27+231151.6	ATEL 7250	ATEL 7250	
	PS15zn		2MASX J10495032+1752553	ATEL 7375	ATEL 7375	Ic
	PS15adh		2MASX J13303174−0044033	ATEL 7431	ATEL 7431	
	PS15ahs	Gaia15afd	MCG +7-37-11	ATEL 7471	ATEL 7477 ATEL 7611	
	PS15aii	Gaia15afk	CGCG 71-25	ATEL 7484	ATEL 7486	
	PS15akf	CSS150519:141711+072139	2MASX J14171303+0721454	ATEL 7519	ATEL 7519	
	PS15asb	CSS150619:142020−091803	Anonymous	ATEL 7683	ATEL 7683	
	PS15atx		2MASX J13031865−2303572	ATEL 7679	ATEL 7679	
	PS15bbn		Anonymous	ATEL 7753	ATEL 7777 ATEL 7832	
	PS15bdr		2MASX J16544931+3643391	ATEL 7785	ATEL 7785	
	PS15bif		Anonymous	ATEL 7832	ATEL 7832	91T
	PS15bjg		2MASX J22551005−0024333	ATEL 7846	ATEL 7846	
	PS15brr	MASTER OT J235325.61−153917.6 PSN J23532561−1539176	GALEXASC J235326.18−153921.5	ATEL 7905	ATEL 7934	91T
	PS15bsq	CSS150918:234152-083816	MCG -02-60-012	ATEL 7937	ATEL 7937	
	PS15bst		GALEXASC J233401.02−131743.5	ATEL 7937	ATEL 7937	

Table 1 – *continued*

IAU name	Discovery name	Alternative names	Galaxy	Discovery ref.	Classification ref.	Type
	PS15bwh		Anonymous	ATEL 8037	ATEL 8037	91T
	PS15bzz	CSS150918:003742+014547 iPTF15cpg	2MASX J00374156+0146014	ATEL 8069	ATEL 8069	
	PS15cfn		GALEXASC J215922.04−210713.3	ATEL 8151	ATEL 8151	91T
	PS15cge		2MASX J23352102+0110271	ATEL 8151	ATEL 8151	
	PS15cku		2MASX J01242239+0335168	ATEL 8200	ATEL 8200	
	PS15cms		2MASX J09583540+0044336	S16	S16	
	PS15cwx		2MFGC 04279	ATEL 8299	ATEL 8300 ATEL 8301	91T
	PS15cze		2MASX J03472342+0052316	ATEL 8363	ATEL 8363	
	PSN J01534240+2956107		UGC 1359	TOCP	ATEL 8506	
	PSN J02524671+4656470		UGC 2351	TOCP	ATEL 8081	
	PSN J08593491+4555343	Gaia15acx PS15tb	UGC 4709	TOCP	ATEL 7222 ATEL 7234	
	PSN J12040516+1404059	Gaia15agh	CGCG 69-37	TOCP	ATEL 7641 ATEL 7556	
	PSN J16025128+4713292	PS15aoq	UGC 10156	TOCP	ATEL 7544 ATEL 7611	
	PSN J16283836+3932552	PS15aot	NGC 6166	TOCP	ATEL 7528 ATEL 7533	91bg
	PSN J20435314+1230304		NGC 6956	TOCP	ATEL 7796	
	PSN J23102264+0735202	PSN J23101633+0732493	NGC 7499	TOCP	ATEL 8016	06gz
	PSN J23523718+1433092	PS15cut	UGC 12822	TOCP	ATEL 8081	

Note. S16 = Smartt et al. (2016).
[a]SN 2017po is hosted by a galaxy pair. It is physically closer to the smaller galaxy, CGCG 223-033 NED01, but we consider it to be more likely to be hosted by the larger galaxy, UGC 10166.

Table 2. PS1 Photometry.

MJD	Filter	Magnitude[a]	Uncertainty	Flux[b]	Uncertainty
		2015I			
57147.250	g_{P1}	14.999	0.004	100 070.0	398.2
57153.254	g_{P1}	14.180	0.004	212 910.0	713.3
57160.258	g_{P1}	14.126	0.004	223 670.0	751.7
57167.258	g_{P1}	14.502	0.005	158 270.0	700.7
57147.250	r_{P1}	14.953	0.004	104 410.0	351.0
57153.254	r_{P1}	14.190	0.003	210 800.0	624.9
57160.258	r_{P1}	14.056	0.003	238 630.0	642.7

Note. Full table is available online.
[a]Limiting magnitudes are 3 σ.
[b]Flux units are such that $m = 27.5–2.5\log_{10}(f)$.

of an SN Ia is correlated with its near-maximum light ejecta velocity. Since there is a broad and skewed SN Ia intrinsic colour distribution, an incorrectly assumed intrinsic colour will result in an incorrect reddening estimate, and thus an incorrect distance measurement. Therefore, measuring the ejecta velocity removes a potential bias in cosmological analyses. While it is unlikely that every Foundation SN will have a measured near-maximum ejecta velocity, precisely measuring the distribution is sufficient for debiasing all SNe in the sample (however those with velocity measurements will have more precise distances).

SN host-galaxy data can improve distance measurements and reduce a potential systematic bias. After making all light-curve shape corrections, there remains a trend between Hubble residuals and host-galaxy properties such as stellar mass and metallicity (e.g. Kelly et al. 2010; Lampeitl et al. 2010; Sullivan et al. 2010; Pan et al. 2014). Since the Foundation Supernova Survey draws its sample primarily from untargeted surveys, there is no inherent bias towards massive host galaxies (unlike previous low-z samples). Recent cosmological analyses have removed this trend (e.g. Betoule et al. 2014); however, the exact size of the effect, its functional form with host-galaxy parameters such as mass (e.g. a step function, a linear trend, etc.), if there is evolution with redshift, and its physical cause are all currently unknown. None the less, it is clear that having these data are critical for making the best cosmological measurements.

With PS1, we already have sufficiently deep $grizy_{P1}$ imaging for nearly every host galaxy. From these data alone, we can determine properties such as stellar mass and SFR to reasonable precision. To these data, we will add *GALEX* UV, 2MASS NIR, and *WISE* IR measurements when possible. For the current Foundation sample, the vast majority of host galaxies have detections and/or constraining limits in these data sets. With these broad-wavelength coverage SEDs, the Foundation host galaxies will have very precisely measured parameters.

NIR light curves provide a path to smaller distance scatter than obtained with only optical light curves (Mandel et al. 2009; Dhawan, Jha & Leibundgut 2017). This is because of a combination of lower dust extinction (resulting in a smaller error from extinction corrections) and a theoretically predicted smaller luminosity scatter in these bands (Kasen & Woosley 2007). While the y_{P1} band, with a central wavelength of 0.96 μm, technically covers some NIR wavelengths, observations in *JHK* bands both extend the lever-arm for extinction measurements and provide information that is relatively uncorrelated from the optical (Mandel et al. 2011). We have begun coordinating with multiple groups to obtain NIR light curves of a subset of Foundation SNe. Although only a relatively small subset of Foundation SNe will have NIR light curves, this subsample may be particularly important for determining the reddening distribution of the full sample as well as being a high-fidelity training sample for *WFIRST*.

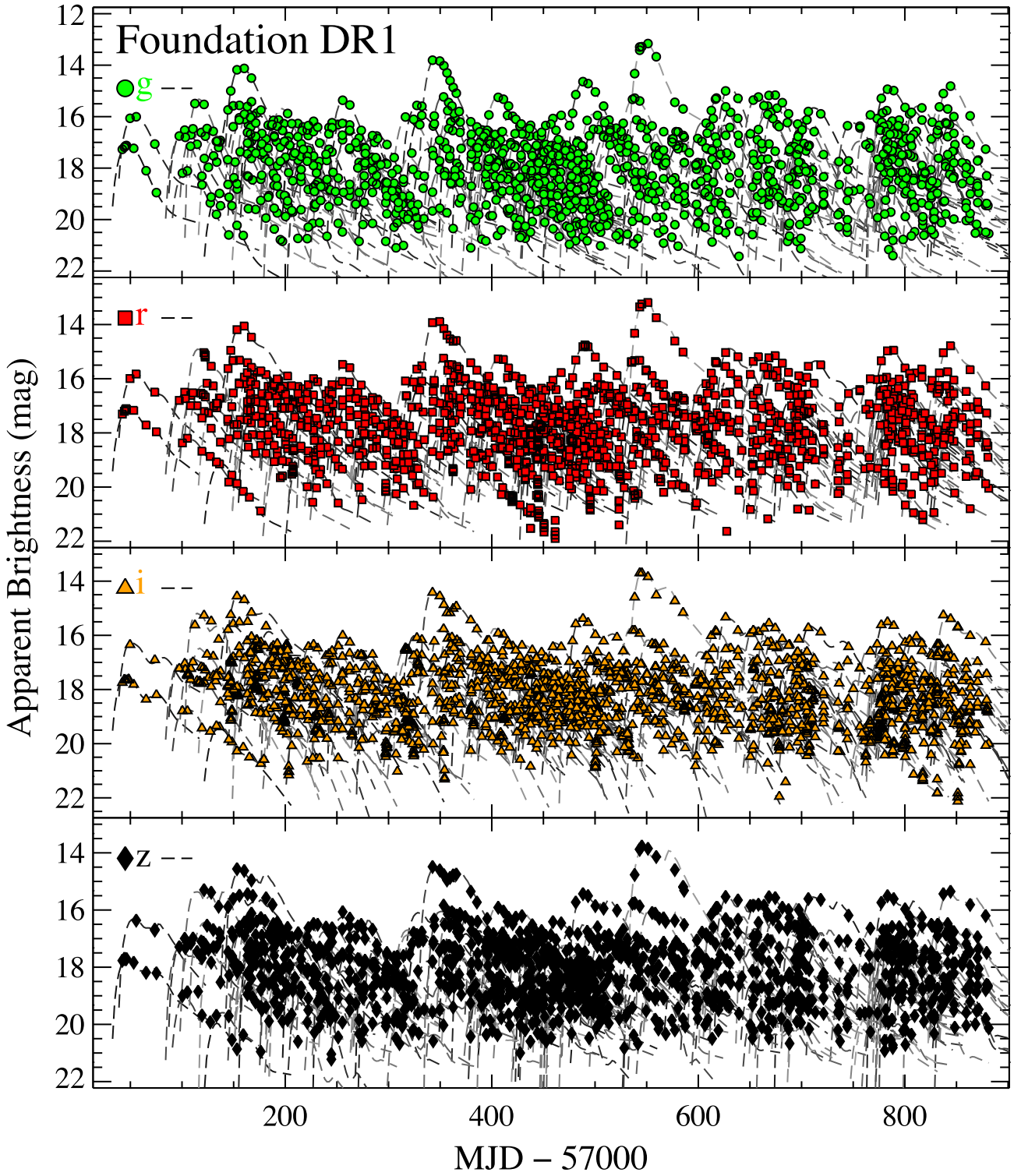

Figure 6. Multicolour light curves for the Foundation DR1 sample. The $griz_{P1}$ photometry are plotted as green circles, red squares, orange triangles, and black diamonds, respectively. The grey lines are SALT2 model fits to each SN light curve.

5 RESULTS

5.1 Classifications and redshifts

Every SN presented in DR1 has been classified as an SN Ia. References for initial classifications are listed in Table 1. For those objects where we have access to a spectrum, either from our own observations, through public surveys such as the Public ESO Spectroscopic Survey for Transient Objects Survey (PESSTO; Smartt et al. 2015), or through services such as the Transient Name Server (TNS), we examined each spectrum individually. Usually, the initial classifications are consistent with our classifications, but on occasion there are differences in subclassification and/or

redshift determination. We present those objects and the differences below.

Since the Foundation SN sample is drawn primarily from untargeted surveys, many SNe in our sample do not have a catalogued host-galaxy redshift. To determine the redshifts for all objects, we take a tiered approach. First, we use redshifts from public surveys with precise redshifts, which is possible for ∼70 per cent of all SNe in our sample. Secondly, we use our redshifts measured from our own spectra of the host-galaxy nucleus. Thirdly, we use redshifts determined from our own spectra host-galaxy features at the SN position (usually present in the SN spectrum). Fourthly, we use redshifts from host-galaxy features from public SN spectra. Fifthly, we use the SN spectra to determine a redshift. Finally, if necessary, we use redshifts reported by other groups. We detail this process below.

For all objects where there was an easily identified host galaxy, we used the NASA/IPAC Extragalactic Database (NED) to determine if there is a host-galaxy redshift. For those with multiple redshift measurements, we chose the one with the smallest uncertainty. A small subset of objects (e.g. ASASSN-15nq) have host-galaxy redshifts in other catalogues (for ASASSN-15nq, the galaxy has an SDSS spectrum), and we use those sources when necessary.

When no catalogued galaxy redshift is available, we first use our own host-galaxy spectra, which are generally obtained when observing an SN, to measure a redshift. Occasionally, host-galaxy emission or absorption features are present in the SN spectrum itself, and we are able to measure a redshift from those. When possible, we obtain our own spectrum of the host-galaxy nucleus, often after the SN has faded. Rarely, other groups will report an otherwise unknown host-galaxy redshift when classifying an SN, and we use those data when appropriate.

After all attempts to obtain a host-galaxy redshift are made, there remain a number of SNe for which we must rely on the SNe themselves for a redshift (currently 5 SNe, or 2.3 per cent of the sample). When we have access to a spectrum, we use the SuperNova IDentification (SNID) software (Blondin & Tonry 2007) to cross-correlate with SN Ia templates and determine the redshift (see e.g. Foley et al. 2009; Rest et al. 2014).

As a last resort, we use redshift estimates from SN spectra as presented in classification announcements. For all direct measurements, we either use the reported redshift uncertainties or measure them ourselves. For reported host-galaxy and SN redshifts, we assume uncertainties of 0.001 and 0.01, respectively. We present newly measured redshifts in Table 3. In total, the host galaxies for 70 SNe Ia in our sample (32.7 per cent) did not have a catalogued redshift, a surprisingly high fraction.

All SN spectra obtained by our group will be presented in a future analysis. For the subset of SNe where either our redshift or classification differs substantially from the initial classification, we present those differences in Tables 4 and 5, respectively. For 21 (4) SNe, corresponding to 9.3 per cent (1.9 per cent) of our sample, the differences between the initially reported redshift and our adopted redshift is large enough to produce a distance modulus bias of >0.3 mag (>1 mag). Host-galaxy redshifts are critical to reduce the scatter of low-z SN Ia samples; the Foundation Supernova Survey is currently 97.7 per cent complete.

5.2 Light-curve parameters

While there are currently several algorithms for estimating distances from SN light curves (e.g. MLCS, Jha, Riess & Kirshner 2007; SiFTO, Conley et al. 2008; BayeSN, Mandel et al. 2009, 2011; SNooPy, Burns et al. 2011; BaSALT, Scolnic et al. 2014a), currently the most widely used light-curve fitting algorithm is SALT2 (Guy et al. 2007). This algorithm is based on SALT (Guy et al. 2005) and assumes a Tripp (1998) parametrization,

$$\mu_B = m_B - M + \alpha x_1 - \beta c, \tag{3}$$

where μ_B, the distance modulus, is determined for each SN given observables m_B, the peak B-band brightness, x_1, a light-curve shape parameter, and c, an observed colour parameter. The parameters M, α, and β are nuisance parameters that are globally fit. One can consider α and β to be the linear slopes between absolute magnitude and light-curve shape and colour, respectively. Meanwhile, M is the B-band absolute magnitude of a fiducial SN Ia with $x_1 = c = 0$.

We use the most recent version of SALT2 (Guy et al. 2010) as implemented in SNANA (Kessler et al. 2009). When fitting light curves, we follow the procedure of Rest et al. (2014), and we refer the reader there for more details. After an initial fit, we remove any suspicious photometry points from each light curve. We identify such points as having $\chi^2 > 10$ relative to the best-fitting SALT2 model. This cut is similar to that done by Holtzman et al. (2008) and Rest et al. (2014). We visually inspected many of the epochs with bad photometry and found a high correlation with image streaks and other subtraction artefacts, indicating that these data are generally poor rather than an issue with the data reduction or model. In total, 81 out of 6868 data points (1.2 per cent), averaging 0.36 data points per SN, were removed. We present the parameters which result from light-curve fitting in Table 6.

5.3 Sample cuts

When targeting specific SNe, we only required that the SN should be spectroscopically confirmed as a young SN Ia with $0.015 < z \lesssim 0.08$. As a result, we include some SNe Ia that are spectroscopically peculiar and have relatively high host-galaxy reddening. We are hopeful that these SNe will be cosmologically useful in the future, but such SNe are not well fitted by SALT2, and must be culled from our current cosmology sample.

Our cosmology sample is set using a combination of criteria defined by Rest et al. (2014) and Betoule et al. (2014). We list the criteria below, but refer the reader to previous works for additional details. The criteria are as follows:

(i) The SN is not spectroscopically similar to SNe Iax (Foley et al. 2013; Jha 2017), SN 1991bg (Filippenko et al. 1992; Leibundgut et al. 1993), the peculiar SN 2000cx (Li et al. 2001), and the high-luminosity SN 2006gz (e.g. Howell et al. 2006; Hicken et al. 2007; Yamanaka et al. 2009; Silverman et al. 2011; Taubenberger et al. 2011; Scalzo et al. 2012).
(ii) The Milky Way reddening towards the SN is $E(B-V)_{\rm MW} < 0.25$ mag.
(iii) At least 11 total light-curve points in $gri_{\rm P1}$.
(iv) The first light-curve point has a phase of $<+7$ d.
(v) The uncertainty on x_1 is <1.
(vi) The uncertainty on the time of peak brightness is <1 d.
(vii) $-0.3 < c < 0.3$.
(viii) $-3.0 < x_1 < 3.0$.
(ix) Chauvenet's criterion applied to the pulls (rather than the residuals, which would bias against the lowest redshift SNe with larger peculiar velocity scatter) to exclude systematic outliers.

The first criterion is to remove spectroscopically peculiar SNe which may be poorly fit by SALT2 or do not follow the width–luminosity

Table 3. Uncatalogued redshifts.

SN	Galaxy	Redshift	Redshift uncertainty	Derived from	Telescope /ATEL[a]
2016E	2MASX J05034387+0324429	0.052 73	0.000 02	nucleus	SOAR
2016J	Anonymous	0.026 42	0.000 06	nucleus	KPNO
2016afb	Anonymous	0.0677	0.0010	SN position	KPNO
2016ajl	2MASX J04422451−2143312	0.067 41	0.000 05	nucleus	SOAR
2016alt	GALEXASC J063701.16+441611.9	0.090	0.006	SN	UH 2.2-m
2016aqb	2MASXi J1121579−135849	0.062 89	0.000 04	nucleus	KPNO
2016aqs	Anonymous	0.025 07	0.000 03	nucleus	KPNO
2016asf	KUG 0647+311	0.018 019	0.000 015	nucleus	KPNO
2016ayg	SDSS J073017.25+250153.5	0.042 69	0.000 12	nucleus	KPNO
2016bfc	Anonymous	0.0478	0.0002	nucleus	Keck I
2016bkw	SDSS J115949.80+544807.1	0.077 720	0.000 099	SN position	KPNO
2016blc	GALEXASC J104848.62−201544.1	0.012 85	0.000 10	nucleus	KPNO
2016blg	SDSS J132713.81−021615.2	0.061 08	0.000 12	nucleus	SOAR
2016blm	Anonymous	0.030 64	0.000 04	nucleus	SOAR
2016bmh	GALEXASC J133213.24+844042.7	0.023 02	0.000 09	nucleus	ARC
2016ccj	SDSS J171023.63+262350.3	0.041 376	0.000 014	nucleus	Keck I
2016cck	2MASX J17353788+0848387	0.035 57	0.000 02	SN position	FLWO 1.5-m
2016cuv	GALEXASC J161914.56+402512.5	0.083 20	0.000 17	nucleus	ARC
2016cxb	GALEXASC J211223.05+144644.9	0.029 54	0.000 09	nucleus	SOAR
2016dxv	Anonymous	0.024 31	0.000 16	nucleus	Keck I
2016eee	SDSS J132307.25+523858.1	0.030 29	0.000 15	nucleus	KPNO
2016eja	2MASX J22253147+3859010	0.030 858	0.000 008	nucleus	KPNO
2016eky	2MASX J22593744+0209095	0.051 27	0.000 03	nucleus	KPNO
2016enx	GALEXASC J011422.73−130915.9	0.071 80	0.000 06	nucleus	SOAR
2016eoa	NGC 83	0.021 09	0.000 07	nucleus	KPNO
2016fbo	GALEXASC J010135.75+170604.9	0.030 46	0.000 09	nucleus	SOAR
2016gfr	2MASX J18193566+2347137	0.016 69	0.000 12	nucleus	Keck I
2016glp	GALEXASC J233613.95+234146.7	0.084 93	0.000 12	nucleus	SOAR
2016glz	GALEXASC J000556.57+082613.6	0.040 10	0.000 07	SN position	SOAR
2016gmb	GALEXASC J003445.02−060936.8	0.058 27	0.000 08	nucleus	SOAR
2016gou	Anonymous	0.0155	0.0010	SN position	Faulkes-North/ATEL 9549
2016grz	SDSS J015533.01+334921.3	0.0875	0.0005	nucleus	KPNO
2016gsn	2MASXi J0229172+180515	0.015 05	0.000 04	nucleus	SOAR
2016gsu	SDSS J010824.54+210906.3	0.076 42	0.000 06	SN position	FLWO 1.5-m
2016hot	SDSS J015319.55+171854.5	0.079	0.003	SN	MDM/ATel 9695
2016hpw	Anonymous	0.021 17	0.000 18	nucleus	Keck I
2016hpx	GALEXASC J060226.54−265949.2	0.0334	0.0005	SN position	NTT/ATel 9704
2016hjk	2MASX J02314347−2500088	0.085 27	0.000 15	nucleus	SALT
2016ick	SDSS J000702.87−204150.1	0.052 50	0.000 10	nucleus	SALT
2016idy	GALEXASC J013415.00−174836.1	0.044 85	0.000 04	nucleus	SOAR
2016iyv	GALEXASC J090013.19−133803.5	0.031	0.002	SN	NTT/ATel 9889
2016ixf	SDSS J103944.53+150204.7	0.066 02	0.000 11	SN position	Keck I
2016jem	Anonymous	0.049 37	0.000 13	SN position	SOAR
2017dz	SDSS J082425.68+245951.5	0.092	0.010	SN	TNG/GCN 20408
2017lc	Anonymous	0.060	0.002	SN	NOT/ATel 9990
2017lm	2MASX J03013238−1501028	0.030 64	0.000 06	nucleus	SALT
2017mu	GALEXASC J093036.72+212437.4	0.0816	0.0004	SN position	LJT/ATel 10018
2017ns	2MASS J02491020+1436036	0.0288	0.0004	SN position	Copernico/ATel 9996
2017nw	Anonymous	0.076 96	0.000 07	nucleus	Keck I
2017wb	2MASX J11011991+7039548	0.030 65	0.000 08	SN position	Faulkes-North
2017adj	Anonymous	0.031 65	0.000 10	nucleus	Keck I
2017ckf	Anonymous	0.047 67	0.000 11	nucleus	Keck I
2017coa	SDSS J084955.19+560554.6	0.040	0.003	SN	BAO 2.16-m/ATel 10235
ASASSN-15bm	GALEXASC J150551.56−053737.2	0.020 43	0.000 10	nucleus	SOAR
ASASSN-15hy	Anonymous	0.0179	0.0002	nucleus	Keck I
ASASSN-15rw	GALEXASC J021558.44+121415.2	0.018 84	0.000 07	SN position	FLWO 1.5-m
ASASSN-15sf	GALEXASC J001127.51−062549.8	0.0247	0.0010	nucleus	KPNO
ASASSN-15ti	2MASX J03051061+3754003	0.017 32	0.000 05	nucleus	KPNO
CSS151120:044526-190158	Anonymous	0.0719	0.0006	nucleus	SOAR
iPTF17fs	Anonymous	0.108	0.005	SN	GTC/GCN 20409
PS15mt	SDSS J095444.27+231151.6	0.070 85	0.00009	SN position	Keck II
PS15ahs	MCG +7-37-11	0.025 51	0.00004	nucleus	SOAR
PS15asb	Anonymous	0.0486	0.0003	nucleus	Keck I

Table 3 – *continued*

SN	Galaxy	Redshift	Redshift Uncertainty	Derived From	Telescope /ATEL[a]
PS15atx	2MASX J13031865−2303572	0.0719	0.0003	SN position	SALT
PS15bbn	Anonymous	0.037 10	0.00012	nucleus	Keck I
PS15bif	Anonymous	0.0794	0.0003	SN position	SOAR
PS15brr	GALEXASC J235326.18−153921.5	0.051 80	0.00009	nucleus	SOAR
PS15bst	GALEXASC J233401.02−131743.5	0.088 50	0.00017	SN position	SOAR
PS15bwh	Anonymous	0.0727	0.0004	nucleus	Keck I
PS15cfn	GALEXASC J215922.04−210713.3	0.1106	0.0015	SN position	SOAR
PS15cku	2MASX J01242239+0335168	0.023 27	0.00007	SN position	SOAR
PS15cwx	2MFGC 04279	0.030 06	0.00011	nucleus	SOAR

[a] If just a telescope is listed, the spectrum was obtained by us and (re-)analysed for this study. If just an ATEL is listed, we simply list the redshift reported in that ATEL. If both a telescope and ATEL are listed, we analysed the publicly available spectrum, which was either submitted to TNS or WISERep, and report our derived redshift.

Table 4. Significant redshift differences.

SN	Reported z	Updated z	Absolute z difference	μ Bias (mag)
2016J	0.034	0.026 4217	0.007 5783	0.560
2016aqs	0.03	0.025 0655	0.004 9345	0.398
2016asf	0.021	0.018 0194	0.002 9806	0.337
2016blg	0.07	0.061 0813	0.008 9187	0.310
2016cck	0.041[a]	0.035 57	0.005 43	0.317
2016cvv	0.038	0.044 5710	0.006 571	− 0.357
2016eee	0.026	0.030 29	0.004 29	− 0.339
2016gfr	0.014	0.016 693	0.002 693	− 0.386
2016glz	0.02	0.040 9939	0.020 9939	− 1.592
2016gsn	0.018	0.015 0541	0.002 9459	0.393
2017jl	0.02	0.016 3310	0.003 669	0.446
2017lc	0.05	0.060[b]	0.01	− 0.411
2017cfc	0.03	0.024 0270	0.005 973	0.492
2017cgr	0.037	0.030 5840	0.006 416	0.424
2017cii	0.04[c]	0.033 2378	0.006 7622	0.413
ASASSN-15hy	0.025	0.017 93	0.007 07	0.733
iPTF17fs	0.068	0.108	0.040	− 1.06
PS15ahs	0.03	0.025 5129	0.004 4871	0.359
PS15asb	0.03	0.048 6300	0.018 63	− 1.079
PS15cwx	0.046	0.0301	0.0159	0.946
	0.055		0.0249	1.348
PSN J23102264+0735202	0.046	0.039 15	0.006 85	0.361

[a] Piascik & Steele (2016) initially reported a redshift of 0.04, but Zhang et al. (2016) reported a redshift of 0.037, which is only moderately different from our measured value of 0.035 57.
[b] The SN is most similar to SN 2000cx (Li et al. 2001) at $z = 0.060 \pm 0.002$. However, it is also somewhat similar to SN 1991bg-like objects at $z = 0.047 \pm 0.007$.
[c] Fraser et al. (2017) initially reported a redshift of 0.04, but Morrell et al. (2017) reported an NED redshift of 0.033 253, which is only slightly different from our preferred value of 0.033 2378.

relation (Phillips 1993). The next three criteria are light-curve quality cuts, which help ensure that the resulting parameters are reasonable and reduce the number of unreliable light-curve fits. The fourth and fifth criteria are the bounds of the SALT2 model. The final criterion excludes systematic outliers that are far from a normal distribution. The SNe passing all of these criteria compose the Foundation 'cosmology' sample. Table 7 displays how each criterion affects our sample as well as the cumulative effect of the criteria.

Upon closer inspection of spectra for our sample, we have determined that PS15zn is likely an SN Ic rather than an SN Ia (Pan et al. 2015a). We therefore exclude the SN from our cosmology sample, but still include its photometry here.

We have decided to observe SNe similar to SNe 1991bg and 2006gz, knowing that SALT2 cannot properly fit their light curves. We note that for the former case, this is not because the SNe are inherently uncalibratable; for instance, MLCS (Riess, Press & Kirshner 1996; Jha, Riess & Kirshner 2007) is able to obtain reasonable distances for SN 1991bg-like objects. Rather than potentially bias the sample because of a classification by other groups or our current ability to properly estimate distances to particular subclasses of SNe Ia, we have decided to photometrically follow this small subset of SNe, and remove them from any current cosmological analysis. Based on public classifications and our own spectra, we designate ASASSN-15ga, MASTER OT J222232.87−185224.3, PSN J16283836+3932552, SN 2016ajf, and SN 2016arc as similar to SN 1991bg and ASASSN-15hy, PSN J23102264+0735202, SN 2015M, SN 2016alt, 2016ccj, and 2017mu as similar to SN 2006gz. These objects represent 5.3 per cent of our total sam-

Table 5. Classification differences.

SN	Reported class.	Updated class.
2015M	SN 1991T-like	SN 2006gz-like
2016aex	SN 1991T-like?	SN 1991T-like
2016alt	Normal	SN 2006gz-like
2016aqa	Normal	SN 1991T-like
2016aqb	Normal	SN 1991T-like
2016arc	Normal	SN 1991bg-like
2016ayf	Normal	SN 1991T-like
2016enx	SN 1991T-like?	SN 1991T-like
2017jl	Normal	SN 1991T-like?
2017lc	Normal	SN 2000cx-like?; SN 1991bg-like?
2017mu	Normal	SN 2006gz-like
PS15zn	SN Ia	SN Ic
PS15bwh	Normal	SN 1991T-like
PS15cwx	SN 1991T-like	Normal[a]
PSN J23102264+0735202	Normal	SN 2006gz-like[b]

[a]Spectrum provided by C. Kilpatrick, private communication.
[b] Elias-Rosa et al. (2015) remark that at the nominal host redshift the SN would have a low Si II ejecta velocity, and suggest that the host galaxy was misidentified. However, the spectrum is more consistent with SN 2006gz at the nominal redshift (see also Table 4).

ple, but notably, ASASSN-15ga, ASASSN-15hy, and MASTER OT J222232.87−185224.3 would have been excluded by other criteria.

Only three objects were cut because of insufficient light-curve coverage. One, ASASSN-15bm, was observed during our pre-survey stage, making it a special case. Of the remaining criteria, none affects more than 5 per cent of the sample. In total, we lose 15.6 per cent of our sample to various cuts, but only 10.8 per cent of the 'normal' SNe Ia. While we hope to improve this number as the survey progresses, the Foundation Survey is already extremely efficient relative to other low-z surveys. For instance, 54 per cent, 54 per cent, and 47 per cent of the CfA3, CfA4, and CSP samples (Hicken et al. 2009a, 2012; Contreras et al. 2010) were cut from the Rest et al. (2014) cosmology sample. Rather, the Foundation sample has a similar fraction of SNe excluded from high-z samples such as SDSS (26 per cent; Betoule et al. 2014; Sako et al. 2014) and PS1 (24 per cent; Rest et al. 2014).

5.4 Sample demographics

Fig. 7 displays the redshift, light-curve shape (x_1), and observed colour (c) distributions of the Foundation sample compared to the existing low-z sample (as prepared by Scolnic et al. 2017). For the Foundation sample, we present the results for the full sample and the cosmology sample, which pass the various criteria listed in Section 5.3.

The low-z SN light curves were fitted with the same version of SALT2 and values for the nuisance parameters to give a consistent comparison. We note that the low-z sample has already been culled of SNe that do not pass various quality cuts which are similar to those employed for the Foundation sample. The Foundation cosmology sample has relatively similar demographics to the existing low-z cosmology sample. The Foundation cosmology and existing low-z samples have similar median redshifts (0.033 compared to 0.029) and median colour (−0.021 compared to −0.035). However, the typical light-curve shapes are different with median values of $x_1 = -0.203$ and 0.160 for the Foundation and existing low-z sample, respectively. The Foundation x_1 distribution does not have the double-peaked distribution seen in the existing low-z sample.

The most striking feature is the relative excess of slow-declining SNe for the Foundation sample. While this may be caused by selection effects (of either Foundation or the other low-z surveys), issues with fitting the Foundation light curves, or statistical fluctuations, it does not appear to be a significant issue for measuring cosmological parameters. Regardless, we will revisit this issue with future data releases.

We note that 18.4 per cent and 3.0 per cent of the Foundation SN sample has been classified as being similar to SN 1991T (or SN 2006gz) and SN 1991bg, respectively. These fractions are similar to the magnitude-limited fractions found by Li et al. (2011) of 17.7 per cent and 3.3 per cent, respectively.

5.5 Hubble diagram

Using the measured distance moduli and redshifts for the Foundation cosmology sample, we present a Hubble diagram in Fig. 8. Although the scatter in the Hubble diagram is small, we caution using the current data in more detailed cosmological analyses at this time. We have not yet produced a robust systematic analysis or determined accurate distance bias corrections (e.g. from Malmquist bias; these are typically up to ∼0.02 mag; Scolnic et al. 2017). Similarly, we have not measured the necessary host-galaxy properties to obtain the precise distances required for such work.

None the less, the Foundation sample Hubble residuals relative to a fiducial ΛCDM model are encouraging. Fitting a Gaussian function to the residuals, we find a standard deviation of only 0.138 mag. We also measure a weighted root-mean square (rms) of 0.136 mag for the Hubble residuals, consistent with the simple Gaussian measurement. Similarly, fitting a Gaussian function to the pulls (the residual divided by the uncertainty), we find a standard deviation of 1.60, close to the expected value of 1 for a normal distribution with uncertainties exactly matching the full scatter. Since the standard deviation of the pull is larger than 1, there must be an additional term, such as intrinsic scatter, that is currently not included in the uncertainties. We plot these distributions in Fig. 9.

In addition to the relatively small Hubble residuals, we find an intrinsic scatter of only $\sigma_{\rm int} = 0.111$ mag, when we require that $\chi^2/{\rm dof} = 1$. A smaller value of $\sigma_{\rm int} = 0.105$ mag is found when requiring that the standard deviation of the pulls be 1. Further improvements to our data reduction pipeline, the PS1 calibration, the available extant data, and the distance-fitting algorithm/model should all improve the intrinsic scatter.

Despite the current success, there are still several aspects that require additional future scrutiny. In particular, there is a moderate correlation between the absolute Hubble residuals and the redshift uncertainty. SNe with precise redshifts ($dz < 10^{-3}$) have median absolute Hubble residuals that are significantly smaller than of SNe with less precise redshifts ($dz \geq 10^{-3}$): 0.086 and 0.119 mag, respectively. We expect that more precise redshifts will improve the distance residuals for the latter group of SNe and will likely decrease the measured intrinsic scatter and rms of our sample.

Finally, we note that eight of the nine SNe Ia that do not pass Chauvenet's criterion have Hubble residuals of $d\mu \approx -0.5$ mag. Six of these objects (SNe 2016ai, 2016aqa, 2016aqt, 2016ayf, 2016hjk, and CSS151120:044526-190158) have spectra that are possibly consistent with SN 2006gz and other high-luminosity, peculiar SNe Ia. Additionally, these SNe have colour-corrected absolute magnitudes ($M_B = m_B - \beta c - \mu$) of −19.81 to −20.20 mag with a median of −20.06 mag, while the median for the

Table 6. Foundation sample light-curve parameters.

SN	$z_{\rm helio}$	$z_{\rm CMB}$	Peak MJD	x_1	c	m_B (mag)
2015I	0.007 59 (0.000 01)	0.008 75 (0.000 01)	57157.10 (0.14)	− 0.20 (0.19)	0.035 (0.032)	13.67 (0.05)
2015M	0.023 16 (0.000 17)	0.022 81 (0.000 17)	57168.67 (0.13)	0.42 (0.08)	0.005 (0.027)	15.24 (0.03)
2015ar	0.017 00 (0.000 04)	0.016 35 (0.000 04)	57352.05 (0.17)	− 1.96 (0.19)	− 0.092 (0.038)	14.77 (0.06)
2015az	0.020 12 (0.000 10)	0.021 33 (0.000 10)	57362.09 (0.15)	0.13 (0.08)	0.018 (0.036)	14.90 (0.10)
2016E	0.052 73 (0.000 02)	0.053 18 (0.000 02)	57392.44 (0.21)	− 0.09 (0.17)	− 0.055 (0.035)	17.41 (0.06)
2016F	0.016 13 (0.000 01)	0.015 13 (0.000 01)	57406.45 (0.09)	0.21 (0.07)	0.010 (0.028)	14.88 (0.04)
2016H	0.046 11 (0.000 01)	0.047 48 (0.000 01)	57400.28 (0.21)	− 0.63 (0.11)	0.003 (0.028)	17.42 (0.04)
2016J	0.026 42 (0.000 06)	0.027 20 (0.000 06)	57400.64 (0.16)	0.54 (0.13)	0.067 (0.041)	16.05 (0.14)
2016K	0.030 75 (0.000 08)	0.030 12 (0.000 08)	57401.90 (0.03)	− 1.76 (0.14)	− 0.018 (0.033)	16.41 (0.04)
2016W	0.019 25 (0.000 07)	0.019 68 (0.000 07)	57417.84 (0.13)	− 1.39 (0.10)	0.061 (0.032)	15.55 (0.05)
2016ac	0.025 67 (0.000 07)	0.028 00 (0.000 07)	57409.34 (0.11)	0.91 (0.15)	0.170 (0.032)	16.41 (0.04)
2016acs	0.055 47 (0.000 01)	0.057 14 (0.000 01)	57434.12 (0.17)	− 0.06 (0.18)	0.044 (0.030)	17.85 (0.04)
2016aew	0.024 93 (0.000 01)	0.025 44 (0.000 01)	57437.86 (0.20)	− 1.67 (0.07)	− 0.053 (0.032)	16.04 (0.04)
2016aex	0.028 52 (0.000 15)	0.029 98 (0.000 15)	57439.76 (0.12)	0.80 (0.10)	− 0.034 (0.035)	16.01 (0.09)
2016afb	0.067 66 (0.001 00)	0.068 34 (0.001 00)	57416.17 (0.66)	0.71 (0.18)	− 0.163 (0.031)	17.51 (0.05)
2016afk	0.045 60 (0.000 01)	0.047 26 (0.000 01)	57440.60 (0.31)	− 0.09 (0.19)	0.063 (0.032)	17.50 (0.05)
2016ah	0.047 81 (0.000 01)	0.049 54 (0.000 01)	57394.93 (0.18)	− 1.24 (0.14)	− 0.037 (0.032)	17.32 (0.04)
2016ai	0.091 73 (0.000 01)	0.092 72 (0.000 01)	57402.08 (0.27)	0.67 (0.17)	0.074 (0.033)	18.42 (0.05)
2016ajf	0.020 31 (0.000 03)	0.021 65 (0.000 03)	57442.32 (0.03)	− 2.92 (0.17)	0.208 (0.045)	16.51 (0.10)
2016ajl	0.067 41 (0.000 05)	0.068 38 (0.000 05)	57442.70 (0.39)	− 1.05 (0.31)	− 0.008 (0.036)	18.11 (0.05)
2016aqa	0.054 59 (0.000 30)	0.056 40 (0.000 30)	57443.02 (0.07)	0.31 (0.18)	0.153 (0.032)	17.61 (0.05)
2016aqb	0.062 89 (0.000 04)	0.063 91 (0.000 04)	57450.48 (0.20)	0.72 (0.20)	− 0.144 (0.031)	17.23 (0.06)
2016aqs	0.025 07 (0.000 02)	0.025 17 (0.000 02)	57456.25 (0.11)	1.18 (0.12)	0.026 (0.029)	15.93 (0.05)
2016aqt	0.050 41 (0.000 01)	0.050 90 (0.000 01)	57454.56 (0.09)	1.15 (0.11)	0.055 (0.029)	16.91 (0.04)
2016aqz	0.026 68 (0.000 01)	0.029 26 (0.000 01)	57454.88 (0.17)	− 0.39 (0.08)	0.295 (0.029)	17.11 (0.04)
2016arc	0.012 73 (0.000 03)	0.010 27 (0.000 03)	57448.52 (0.28)	− 2.49 (0.20)	0.253 (0.049)	16.16 (0.10)
2016asf	0.018 02 (0.000 01)	0.018 92 (0.000 01)	57464.64 (0.16)	0.34 (0.11)	0.038 (0.034)	15.31 (0.08)
2016aud	0.041 91 (0.000 04)	0.043 45 (0.000 04)	57459.79 (0.43)	1.45 (0.16)	0.014 (0.030)	16.82 (0.05)
2016axb	0.039 30 (0.000 01)	0.040 55 (0.000 01)	57461.28 (0.02)	− 0.72 (0.11)	− 0.021 (0.032)	16.90 (0.04)
2016axw	0.054 00 (0.000 01)	0.054 83 (0.000 01)	57461.05 (0.34)	0.81 (0.18)	− 0.139 (0.030)	17.14 (0.04)
2016ayf	0.034 80 (0.000 01)	0.035 83 (0.000 01)	57460.99 (0.03)	− 0.96 (0.14)	0.088 (0.033)	16.62 (0.04)
2016ayg	0.042 69 (0.000 12)	0.043 42 (0.000 12)	57467.61 (0.14)	− 0.18 (0.15)	− 0.117 (0.030)	16.91 (0.04)
2016baq	0.034 86 (0.000 01)	0.036 49 (0.000 01)	57465.05 (0.21)	− 0.70 (0.11)	0.049 (0.030)	16.83 (0.04)
2016bew	0.053 43 (0.000 08)	0.055 04 (0.000 08)	57466.80 (0.21)	− 0.85 (0.20)	0.014 (0.036)	17.68 (0.07)
2016bey	0.073 02 (0.000 02)	0.073 96 (0.000 02)	57452.90 (0.05)	− 1.73 (0.22)	− 0.366 (0.059)	17.30 (0.08)
2016bfc	0.047 79 (0.000 17)	0.048 23 (0.000 17)	57470.02 (0.34)	1.38 (0.18)	− 0.079 (0.029)	16.84 (0.04)
2016bkw	0.077 72 (0.000 10)	0.078 34 (0.000 10)	57434.92 (0.38)	0.57 (0.28)	− 0.148 (0.031)	18.13 (0.04)
2016blc	0.012 85 (0.000 10)	0.014 22 (0.000 10)	57489.87 (0.07)	0.50 (0.07)	− 0.088 (0.028)	14.29 (0.04)
2016blg	0.061 08 (0.000 12)	0.062 17 (0.000 12)	57477.11 (1.08)	− 0.74 (0.26)	0.037 (0.050)	17.97 (0.11)
2016blh	0.023 80 (0.000 21)	0.023 87 (0.000 21)	57480.01 (0.14)	− 1.91 (0.09)	0.401 (0.037)	17.41 (0.06)
2016blj	0.034 66 (0.000 15)	0.034 68 (0.000 15)	57482.77 (0.34)	− 0.26 (0.12)	0.066 (0.030)	16.70 (0.05)
2016blm	0.030 64 (0.000 04)	0.031 20 (0.000 04)	57482.16 (0.18)	− 0.23 (0.12)	− 0.022 (0.046)	16.31 (0.16)
2016bln	0.023 30 (0.000 03)	0.023 61 (0.000 03)	57499.59 (0.09)	1.13 (0.11)	0.004 (0.029)	15.63 (0.04)
2016bmc	0.028 02 (0.000 08)	0.028 04 (0.000 08)	57486.89 (0.52)	− 1.55 (0.15)	− 0.017 (0.048)	16.25 (0.12)
2016bmh	0.023 02 (0.000 09)	0.023 88 (0.000 09)	57500.82 (0.16)	0.60 (0.11)	0.034 (0.034)	15.89 (0.08)
2016bpb	0.062 70 (0.000 21)	0.063 76 (0.000 21)	57487.52 (0.17)	− 1.17 (0.21)	− 0.107 (0.031)	17.70 (0.04)
2016cby	0.024 91 (0.000 01)	0.025 54 (0.000 01)	57511.29 (0.30)	1.23 (0.18)	0.134 (0.030)	16.58 (0.04)
2016ccj	0.041 38 (0.000 01)	0.042 35 (0.000 01)	57524.83 (0.22)	3.03 (0.18)	− 0.022 (0.031)	16.49 (0.04)
2016cck	0.035 57 (0.000 02)	0.035 76 (0.000 02)	57509.46 (0.42)	− 0.10 (0.22)	− 0.088 (0.034)	16.73 (0.07)
2016ccz	0.015 02 (0.000 01)	0.015 41 (0.000 01)	57538.08 (0.09)	0.06 (0.08)	0.072 (0.027)	15.08 (0.04)
2016cob	0.028 90 (0.000 21)	0.030 75 (0.000 21)	57539.86 (0.44)	0.68 (0.17)	− 0.114 (0.029)	15.83 (0.04)
2016coj	0.004 52 (0.000 06)	0.005 80 (0.000 06)	57548.11 (0.11)	− 1.44 (0.08)	− 0.007 (0.031)	12.85 (0.04)
2016cor	0.049 54 (0.000 03)	0.050 92 (0.000 03)	57541.54 (0.26)	− 0.32 (0.22)	0.199 (0.031)	18.14 (0.04)
2016cpy	0.029 20 (0.000 01)	0.029 49 (0.000 01)	57542.34 (0.39)	− 1.34 (0.13)	− 0.041 (0.033)	16.13 (0.05)
2016cuv	0.083 20 (0.000 17)	0.083 53 (0.000 17)	57555.77 (1.09)	− 0.15 (0.50)	− 0.026 (0.042)	18.51 (0.07)
2016cvn	0.013 69 (0.000 12)	0.013 83 (0.000 12)	57554.79 (0.43)	0.22 (0.13)	1.000 (0.047)	17.20 (0.03)
2016cvv	0.044 57 (0.000 40)	0.044 28 (0.000 40)	57558.50 (0.54)	1.21 (0.19)	0.074 (0.034)	17.20 (0.07)
2016cvw	0.038 88 (0.000 09)	0.038 23 (0.000 09)	57559.86 (0.40)	− 1.71 (0.16)	− 0.020 (0.036)	17.01 (0.06)
2016cxb	0.029 54 (0.000 09)	0.029 18 (0.000 09)	57564.47 (0.32)	1.19 (0.12)	− 0.092 (0.031)	16.04 (0.06)
2016cyt	0.030 74 (0.000 09)	0.030 68 (0.000 09)	57580.52 (0.12)	− 1.73 (0.09)	− 0.092 (0.031)	16.12 (0.06)
2016czc	0.050 93 (0.000 01)	0.051 41 (0.000 01)	57582.35 (0.48)	1.35 (0.26)	− 0.091 (0.030)	16.94 (0.04)
2016dxe	0.073 63 (0.000 01)	0.073 87 (0.000 01)	57490.64 (0.07)	0.76 (0.14)	− 0.071 (0.030)	18.01 (0.04)
2016dxv	0.024 31 (0.000 16)	0.024 47 (0.000 16)	57508.59 (0.22)	0.40 (0.10)	− 0.103 (0.031)	15.60 (0.05)
2016eee	0.030 29 (0.000 15)	0.031 12 (0.000 15)	57517.58 (0.23)	0.86 (0.13)	− 0.058 (0.028)	16.16 (0.03)

Table 6 – *continued*

SN	$z_{\rm helio}$	$z_{\rm CMB}$	Peak MJD	x_1	c	m_B (mag)
2016eja	0.030 86 (0.000 01)	0.030 80 (0.000 01)	57597.04 (0.05)	1.14 (0.15)	0.052 (0.035)	16.29 (0.08)
2016eky	0.051 27 (0.000 03)	0.050 17 (0.000 03)	57598.11 (0.32)	0.73 (0.22)	− 0.072 (0.032)	17.27 (0.06)
2016enx	0.071 80 (0.000 06)	0.072 04 (0.000 06)	57609.10 (0.54)	0.32 (0.26)	0.070 (0.032)	18.21 (0.04)
2016eoa	0.021 09 (0.000 07)	0.021 17 (0.000 07)	57615.72 (0.17)	− 1.51 (0.14)	0.015 (0.035)	15.66 (0.06)
2016eqb	0.025 31 (0.000 15)	0.024 77 (0.000 15)	57605.20 (0.39)	− 0.14 (0.10)	0.090 (0.029)	15.97 (0.04)
2016esh	0.044 57 (0.000 03)	0.045 87 (0.000 03)	57613.23 (0.22)	− 1.00 (0.23)	− 0.118 (0.033)	16.83 (0.05)
2016euj	0.017 01 (0.000 10)	0.016 97 (0.000 10)	57619.31 (0.15)	− 1.04 (0.10)	− 0.066 (0.030)	14.99 (0.04)
2016ews	0.045 55 (0.000 01)	0.046 40 (0.000 01)	57619.93 (0.18)	0.96 (0.19)	− 0.157 (0.032)	16.75 (0.05)
2016fbk	0.035 87 (0.000 01)	0.035 71 (0.000 01)	57625.13 (0.15)	− 0.16 (0.12)	0.117 (0.030)	17.13 (0.05)
2016fbo	0.030 46 (0.000 09)	0.029 85 (0.000 09)	57627.02 (0.54)	0.06 (0.13)	− 0.051 (0.032)	16.05 (0.05)
2016fff	0.011 44 (0.000 01)	0.011 23 (0.000 01)	57629.98 (0.23)	− 1.95 (0.15)	− 0.026 (0.039)	14.58 (0.05)
2016ffh	0.018 19 (0.000 01)	0.018 42 (0.000 01)	57630.79 (0.33)	− 0.82 (0.15)	0.020 (0.015)	15.55 (0.03)
2016gfr	0.016 69 (0.000 12)	0.016 71 (0.000 12)	57657.54 (0.20)	0.24 (0.11)	− 0.021 (0.033)	14.61 (0.08)
2016ghq	0.021 40 (0.000 22)	0.021 19 (0.000 22)	57651.89 (0.37)	− 1.50 (0.14)	0.334 (0.038)	16.57 (0.06)
2016gkt	0.050 72 (0.000 15)	0.049 41 (0.000 15)	57644.06 (0.84)	− 1.07 (0.19)	0.042 (0.054)	17.23 (0.11)
2016glp	0.084 93 (0.000 12)	0.084 12 (0.000 12)	57658.73 (0.23)	0.98 (0.36)	0.136 (0.043)	18.85 (0.07)
2016glz	0.040 99 (0.000 07)	0.041 00 (0.000 07)	57664.48 (0.38)	1.21 (0.23)	− 0.015 (0.032)	16.59 (0.06)
2016gmb	0.058 27 (0.000 08)	0.058 56 (0.000 08)	57656.22 (0.93)	1.29 (0.28)	− 0.109 (0.036)	17.30 (0.06)
2016gmg	0.049 44 (0.000 11)	0.048 53 (0.000 11)	57662.19 (0.24)	− 1.85 (0.26)	− 0.051 (0.043)	17.50 (0.09)
2016gou	0.015 52 (0.001 00)	0.015 37 (0.001 00)	57666.57 (0.09)	0.03 (0.09)	0.079 (0.033)	15.35 (0.08)
2016grz	0.087 48 (0.000 50)	0.087 12 (0.000 50)	57670.56 (0.01)	0.86 (0.38)	0.060 (0.038)	18.63 (0.05)
2016gsn	0.015 05 (0.000 04)	0.014 09 (0.000 04)	57671.76 (0.12)	0.90 (0.13)	− 0.070 (0.039)	14.25 (0.12)
2016gsu	0.076 42 (0.000 06)	0.075 82 (0.000 06)	57670.86 (0.02)	− 1.14 (0.26)	− 0.034 (0.036)	18.36 (0.05)
2016gye	0.021 17 (0.000 11)	0.021 70 (0.000 11)	57674.58 (0.20)	− 1.26 (0.16)	− 0.046 (0.034)	15.21 (0.06)
2016hgw	0.023 08 (0.000 03)	0.022 23 (0.000 03)	57689.27 (0.55)	− 2.53 (0.21)	0.111 (0.045)	16.45 (0.11)
2016hhv	0.061 94 (0.000 14)	0.061 18 (0.000 14)	57694.64 (0.28)	− 1.55 (0.20)	− 0.128 (0.040)	17.72 (0.06)
2016hjk	0.085 27 (0.000 15)	0.084 93 (0.000 15)	57686.19 (0.26)	0.75 (0.28)	0.026 (0.037)	18.09 (0.05)
2016hli	0.016 75 (0.000 10)	0.015 53 (0.000 10)	57694.98 (0.60)	− 1.73 (0.23)	0.044 (0.061)	15.18 (0.24)
2016hns	0.038 17 (0.000 06)	0.037 29 (0.000 06)	57697.45 (0.21)	− 1.11 (0.17)	− 0.108 (0.032)	16.62 (0.05)
2016hot	0.079 00 (0.003 00)	0.078 49 (0.003 00)	57695.48 (0.68)	2.07 (0.35)	0.243 (0.036)	17.83 (0.05)
2016hpw	0.021 17 (0.000 18)	0.020 28 (0.000 18)	57703.56 (0.10)	0.79 (0.17)	0.099 (0.050)	15.68 (0.08)
2016hpx	0.033 38 (0.000 46)	0.032 46 (0.000 46)	57703.93 (0.19)	0.66 (0.12)	− 0.031 (0.032)	16.19 (0.04)
2016hqf	0.054 47 (0.000 01)	0.052 25 (0.000 01)	57694.91 (0.66)	1.47 (0.31)	− 0.014 (0.035)	17.40 (0.06)
2016htm	0.043 31 (0.000 15)	0.042 88 (0.000 15)	57702.65 (0.13)	− 0.06 (0.16)	− 0.080 (0.027)	16.85 (0.04)
2016htn	0.053 12 (0.000 15)	0.052 75 (0.000 15)	57701.32 (0.26)	0.14 (0.23)	0.076 (0.031)	17.78 (0.04)
2016hvl	0.013 08 (0.000 01)	0.013 73 (0.000 01)	57711.04 (0.15)	1.22 (0.16)	0.057 (0.063)	14.19 (0.23)
2016ick	0.052 50 (0.000 10)	0.051 23 (0.000 10)	57719.50 (0.15)	0.43 (0.21)	− 0.072 (0.031)	17.28 (0.04)
2016idy	0.044 85 (0.000 04)	0.043 43 (0.000 04)	57665.36 (0.26)	0.46 (0.14)	− 0.083 (0.033)	16.75 (0.05)
2016ixf	0.066 02 (0.000 11)	0.067 07 (0.000 11)	57742.32 (0.71)	0.94 (0.27)	− 0.104 (0.034)	17.78 (0.05)
2016iyv	0.031 00 (0.002 00)	0.031 82 (0.002 00)	57749.96 (0.26)	1.45 (0.17)	− 0.048 (0.031)	15.90 (0.05)
2016jem	0.049 37 (0.000 13)	0.047 97 (0.000 13)	57755.88 (0.25)	2.42 (0.52)	− 0.062 (0.045)	16.74 (0.06)
2016ys	0.028 34 (0.000 01)	0.029 18 (0.000 01)	57416.59 (0.49)	1.01 (0.15)	0.221 (0.032)	16.76 (0.05)
2016zd	0.031 94 (0.000 15)	0.033 07 (0.000 15)	57430.14 (0.13)	0.64 (0.12)	− 0.155 (0.029)	15.89 (0.05)
2017aaa	0.046 81 (0.000 01)	0.047 90 (0.000 01)	57798.77 (0.07)	1.29 (0.19)	− 0.061 (0.033)	16.97 (0.05)
2017adj	0.031 65 (0.000 10)	0.031 46 (0.000 10)	57796.68 (0.23)	− 0.07 (0.12)	− 0.096 (0.033)	16.09 (0.07)
2017awz	0.022 22 (0.000 01)	0.023 27 (0.000 01)	57813.25 (0.14)	0.79 (0.11)	0.034 (0.030)	15.35 (0.04)
2017azk	0.073 39 (0.000 02)	0.074 26 (0.000 02)	57812.12 (0.24)	− 1.10 (0.26)	− 0.057 (0.037)	18.10 (0.06)
2017cfb	0.022 90 (0.000 01)	0.022 76 (0.000 01)	57836.83 (0.28)	1.02 (0.16)	− 0.072 (0.030)	15.28 (0.04)
2017cfc	0.024 03 (0.000 16)	0.024 95 (0.000 16)	57837.56 (0.12)	− 0.88 (0.09)	0.011 (0.028)	15.90 (0.04)
2017cfd	0.012 09 (0.000 16)	0.012 70 (0.000 16)	57843.68 (0.10)	− 0.43 (0.09)	0.058 (0.030)	14.55 (0.04)
2017cgr	0.030 58 (0.000 15)	0.031 07 (0.000 15)	57804.23 (0.96)	− 0.06 (0.18)	0.008 (0.034)	16.34 (0.06)
2017cii	0.033 24 (0.000 01)	0.032 77 (0.000 01)	57837.52 (0.58)	0.38 (0.15)	− 0.089 (0.031)	16.29 (0.06)
2017cju	0.049 24 (0.000 01)	0.050 81 (0.000 01)	57836.81 (0.46)	− 1.43 (0.17)	0.045 (0.034)	17.51 (0.05)
2017cjv	0.059 53 (0.000 14)	0.061 04 (0.000 14)	57839.86 (0.57)	− 1.28 (0.27)	− 0.102 (0.033)	17.69 (0.04)
2017ckd	0.068 28 (0.000 01)	0.068 92 (0.000 01)	57842.91 (0.25)	− 0.81 (0.21)	− 0.030 (0.032)	18.01 (0.04)
2017ckx	0.027 16 (0.000 01)	0.028 35 (0.000 01)	57846.59 (0.59)	1.74 (0.36)	0.007 (0.035)	16.02 (0.05)
2017coa	0.040 00 (0.003 00)	0.040 90 (0.003 00)	57848.77 (0.46)	0.91 (0.28)	− 0.020 (0.036)	16.97 (0.05)
2017cpu	0.054 41 (0.000 01)	0.055 00 (0.000 01)	57847.56 (0.67)	0.74 (0.34)	− 0.072 (0.032)	17.10 (0.04)
2017dz	0.092 00 (0.010 00)	0.092 91 (0.010 00)	57766.82 (0.77)	1.52 (0.63)	0.049 (0.067)	18.93 (0.13)
2017hm	0.021 27 (0.000 11)	0.022 24 (0.000 11)	57773.63 (0.51)	0.42 (0.32)	− 0.056 (0.037)	15.19 (0.05)
2017hn	0.023 85 (0.000 01)	0.025 85 (0.000 01)	57768.06 (0.42)	0.75 (0.21)	− 0.020 (0.032)	15.64 (0.04)
2017jl	0.016 33 (0.000 44)	0.015 24 (0.000 44)	57784.95 (0.11)	0.66 (0.12)	0.003 (0.031)	14.49 (0.05)
2017lc	0.060 00 (0.002 00)	0.061 27 (0.002 00)	57769.98 (1.43)	0.02 (0.44)	− 0.060 (0.052)	18.00 (0.13)
2017lm	0.030 64 (0.000 06)	0.030 17 (0.000 06)	57778.89 (0.42)	1.03 (0.27)	− 0.012 (0.032)	16.14 (0.05)

Table 6 – *continued*

SN	$z_{\rm helio}$	$z_{\rm CMB}$	Peak MJD	x_1	c	m_B (mag)
2017ln	0.025 37 (0.000 01)	0.027 42 (0.000 01)	57777.03 (0.35)	− 1.62 (0.17)	− 0.028 (0.030)	16.15 (0.04)
2017lv	0.028 71 (0.000 03)	0.029 89 (0.000 03)	57776.57 (0.52)	− 1.98 (0.12)	− 0.098 (0.038)	16.28 (0.07)
2017me	0.032 66 (0.000 01)	0.033 93 (0.000 01)	57782.50 (0.08)	1.40 (0.12)	0.172 (0.030)	17.07 (0.04)
2017mf	0.025 61 (0.000 01)	0.025 82 (0.000 01)	57779.10 (0.06)	− 0.09 (0.10)	− 0.012 (0.029)	16.01 (0.04)
2017ms	0.024 48 (0.000 01)	0.025 96 (0.000 01)	57782.34 (0.33)	0.47 (0.18)	− 0.133 (0.029)	15.52 (0.04)
2017mu	0.081 62 (0.000 43)	0.082 47 (0.000 43)	57772.27 (0.07)	0.46 (0.36)	− 0.016 (0.047)	18.67 (0.07)
2017nk	0.034 45 (0.000 01)	0.033 68 (0.000 01)	57775.69 (0.17)	0.42 (0.25)	0.420 (0.046)	17.69 (0.07)
2017ns	0.028 77 (0.000 40)	0.028 38 (0.000 40)	57784.24 (0.23)	− 0.73 (0.22)	0.225 (0.036)	16.82 (0.07)
2017nw	0.076 96 (0.000 07)	0.077 95 (0.000 07)	57777.25 (1.21)	1.38 (0.38)	− 0.035 (0.039)	18.14 (0.07)
2017oz	0.055 69 (0.000 01)	0.056 12 (0.000 01)	57787.76 (0.33)	0.28 (0.25)	− 0.043 (0.031)	17.51 (0.04)
2017po	0.031 83 (0.000 01)	0.032 33 (0.000 01)	57784.34 (0.09)	0.14 (0.11)	− 0.085 (0.029)	16.11 (0.04)
2017wb	0.030 65 (0.000 08)	0.031 10 (0.000 08)	57790.15 (0.21)	1.35 (0.14)	0.060 (0.029)	16.34 (0.04)
2017ya	0.069 96 (0.000 02)	0.069 06 (0.000 02)	57782.68 (0.02)	1.53 (0.80)	0.038 (0.063)	17.73 (0.09)
2017yh	0.020 40 (0.000 02)	0.020 38 (0.000 02)	57791.14 (0.19)	− 0.98 (0.14)	0.072 (0.033)	15.64 (0.06)
2017yk	0.046 44 (0.000 15)	0.046 89 (0.000 15)	57788.89 (0.35)	− 0.69 (0.24)	0.192 (0.033)	17.98 (0.05)
2017zd	0.029 47 (0.000 15)	0.029 10 (0.000 15)	57793.13 (0.12)	0.30 (0.10)	− 0.039 (0.030)	15.89 (0.06)
ASASSN-15bc	0.036 71 (0.000 10)	0.037 95 (0.000 10)	57047.86 (0.16)	0.59 (0.15)	0.053 (0.028)	16.84 (0.04)
ASASSN-15bm	0.020 43 (0.000 10)	0.020 00 (0.000 10)	57054.12 (0.26)	0.81 (0.23)	0.156 (0.034)	15.61 (0.06)
ASASSN-15fa	0.027 35 (0.000 01)	0.027 26 (0.000 01)	57102.10 (0.38)	0.77 (0.18)	0.069 (0.029)	16.29 (0.04)
ASASSN-15fs	0.029 02 (0.000 05)	0.029 20 (0.000 05)	57113.33 (0.20)	0.04 (0.10)	0.015 (0.030)	16.00 (0.06)
ASASSN-15ga	0.006 60 (0.000 01)	0.007 97 (0.000 01)	57115.62 (0.39)	− 2.86 (0.22)	0.387 (0.064)	15.14 (0.07)
ASASSN-15go	0.018 92 (0.000 15)	0.018 68 (0.000 15)	57122.71 (0.10)	2.47 (0.54)	0.244 (0.045)	15.85 (0.10)
ASASSN-15hg	0.029 92 (0.000 01)	0.031 34 (0.000 01)	57131.32 (0.54)	− 1.23 (0.13)	0.008 (0.032)	16.59 (0.05)
ASASSN-15hy	0.017 93 (0.000 22)	0.017 30 (0.000 22)	57153.23 (0.36)	3.25 (0.30)	0.322 (0.041)	15.03 (0.09)
ASASSN-15il	0.023 32 (0.000 15)	0.022 90 (0.000 15)	57161.44 (0.17)	1.22 (0.11)	− 0.081 (0.035)	15.18 (0.10)
ASASSN-15jl	0.034 68 (0.000 01)	0.035 19 (0.000 01)	57165.95 (0.25)	0.40 (0.13)	− 0.069 (0.027)	16.41 (0.03)
ASASSN-15jt	0.023 06 (0.000 01)	0.022 25 (0.000 01)	57169.79 (0.15)	− 2.39 (0.14)	0.179 (0.036)	16.70 (0.04)
ASASSN-15kx	0.018 02 (0.000 08)	0.016 84 (0.000 08)	57191.62 (0.16)	− 1.42 (0.14)	− 0.075 (0.038)	15.35 (0.10)
ASASSN-15la	0.027 82 (0.000 01)	0.028 25 (0.000 01)	57190.11 (0.22)	− 0.96 (0.21)	0.045 (0.030)	16.08 (0.04)
ASASSN-15lg	0.020 15 (0.000 01)	0.020 37 (0.000 01)	57196.42 (0.30)	− 1.24 (0.14)	− 0.089 (0.037)	15.39 (0.05)
ASASSN-15lu	0.035 05 (0.000 01)	0.036 42 (0.000 01)	57199.51 (0.07)	− 0.62 (0.16)	− 0.032 (0.030)	16.76 (0.04)
ASASSN-15mf	0.026 04 (0.000 01)	0.026 88 (0.000 01)	57211.62 (0.18)	− 0.74 (0.10)	− 0.043 (0.030)	15.93 (0.04)
ASASSN-15mg	0.042 78 (0.000 01)	0.044 49 (0.000 01)	57218.09 (0.14)	− 1.55 (0.15)	− 0.032 (0.032)	17.22 (0.04)
ASASSN-15mi	0.034 42 (0.000 01)	0.035 95 (0.000 01)	57221.17 (0.16)	0.60 (0.12)	− 0.000 (0.028)	16.25 (0.04)
ASASSN-15np	0.037 68 (0.000 05)	0.039 13 (0.000 05)	57241.59 (0.65)	− 0.97 (0.22)	0.047 (0.031)	17.05 (0.04)
ASASSN-15nq	0.030 36 (0.000 01)	0.029 96 (0.000 01)	57247.61 (0.14)	− 0.28 (0.12)	− 0.080 (0.030)	16.10 (0.04)
ASASSN-15nr	0.023 21 (0.000 18)	0.023 42 (0.000 18)	57250.11 (0.14)	1.24 (0.18)	0.040 (0.036)	15.56 (0.08)
ASASSN-15od	0.017 60 (0.000 01)	0.017 03 (0.000 01)	57256.47 (0.29)	− 1.09 (0.12)	− 0.101 (0.031)	15.03 (0.04)
ASASSN-15oh	0.016 83 (0.000 11)	0.015 63 (0.000 11)	57255.90 (0.22)	− 1.59 (0.16)	0.043 (0.042)	15.46 (0.09)
ASASSN-15pm	0.048 78 (0.000 15)	0.048 50 (0.000 15)	57277.89 (0.55)	0.40 (0.22)	− 0.095 (0.029)	16.95 (0.04)
ASASSN-15pn	0.038 36 (0.000 01)	0.039 55 (0.000 01)	57279.45 (0.18)	0.55 (0.13)	− 0.039 (0.032)	16.88 (0.06)
ASASSN-15pr	0.033 09 (0.000 15)	0.033 03 (0.000 15)	57283.08 (0.91)	− 0.64 (0.22)	− 0.043 (0.038)	16.65 (0.06)
ASASSN-15py	0.044 73 (0.000 01)	0.045 62 (0.000 01)	57288.86 (0.97)	− 0.00 (0.26)	0.114 (0.043)	17.32 (0.09)
ASASSN-15rw	0.018 84 (0.000 07)	0.018 39 (0.000 07)	57329.44 (0.11)	1.38 (0.10)	− 0.021 (0.035)	14.93 (0.08)
ASASSN-15sb	0.022 71 (0.000 15)	0.022 79 (0.000 15)	57321.22 (0.49)	− 0.98 (0.24)	0.566 (0.059)	16.73 (0.18)
ASASSN-15sf	0.024 68 (0.001 00)	0.024 45 (0.001 00)	57333.24 (0.19)	1.01 (0.14)	− 0.065 (0.030)	15.70 (0.04)
ASASSN-15so	0.007 02 (0.000 01)	0.008 87 (0.000 01)	57345.34 (0.11)	− 0.71 (0.07)	− 0.052 (0.029)	13.46 (0.04)
ASASSN-15ss	0.035 56 (0.000 12)	0.036 18 (0.000 12)	57338.43 (0.14)	0.82 (0.15)	− 0.088 (0.042)	16.33 (0.13)
ASASSN-15tg	0.035 62 (0.000 06)	0.035 40 (0.000 06)	57361.61 (0.04)	1.46 (0.13)	− 0.058 (0.030)	16.23 (0.04)
ASASSN-15ti	0.017 32 (0.000 06)	0.015 94 (0.000 06)	57364.11 (0.16)	− 1.46 (0.10)	− 0.033 (0.037)	15.38 (0.09)
ASASSN-15tz	0.022 86 (0.000 03)	0.024 02 (0.000 03)	57376.16 (0.18)	− 1.53 (0.14)	0.111 (0.041)	16.22 (0.10)
ASASSN-15uu	0.026 78 (0.000 01)	0.026 31 (0.000 01)	57389.59 (0.39)	1.01 (0.18)	0.190 (0.033)	16.28 (0.05)
ASASSN-15uv	0.020 28 (0.000 02)	0.021 61 (0.000 02)	57392.74 (0.09)	0.17 (0.08)	0.273 (0.029)	16.33 (0.04)
ASASSN-15uw	0.030 81 (0.000 15)	0.030 68 (0.000 15)	57393.31 (0.19)	− 0.68 (0.13)	0.085 (0.030)	16.60 (0.04)
ASASSN-17co	0.018 26 (0.000 15)	0.017 81 (0.000 15)	57808.26 (0.19)	− 0.58 (0.14)	0.100 (0.034)	15.31 (0.07)
CSS151120:044526-190158	0.071 92 (0.000 60)	0.072 04 (0.000 60)	57351.38 (0.45)	0.38 (0.23)	− 0.020 (0.020)	17.74 (0.04)
MASTER OT J151647.17+283742.8	0.056 44 (0.000 01)	0.056 72 (0.000 01)	57582.46 (0.75)	− 0.50 (0.28)	0.104 (0.041)	18.17 (0.07)
MASTER OT J222232.87-185224.3	0.023 94 (0.000 09)	0.023 05 (0.000 09)	57183.36 (0.91)	− 2.33 (0.31)	0.702 (0.067)	18.49 (0.12)
PS15adh	0.102 76 (0.000 02)	0.103 87 (0.000 02)	57136.64 (0.80)	− 0.57 (0.47)	− 0.142 (0.043)	18.77 (0.05)
PS15ahs	0.025 51 (0.000 04)	0.025 25 (0.000 04)	57156.82 (0.06)	0.07 (0.07)	− 0.087 (0.027)	15.71 (0.04)
PS15aii	0.046 55 (0.000 01)	0.047 81 (0.000 01)	57159.64 (0.10)	0.13 (0.11)	− 0.072 (0.028)	17.10 (0.04)
PS15akf	0.058 63 (0.000 01)	0.060 40 (0.000 01)	57163.98 (0.42)	− 1.34 (0.18)	0.229 (0.031)	18.15 (0.04)
PS15asb	0.048 63 (0.000 33)	0.050 25 (0.000 33)	57194.17 (0.17)	− 1.39 (0.17)	− 0.009 (0.034)	17.41 (0.05)
PS15atx	0.071 88 (0.000 27)	0.073 04 (0.000 27)	57192.98 (0.70)	− 1.61 (0.59)	− 0.165 (0.048)	18.17 (0.08)

Table 6 – *continued*

SN	$z_{\rm helio}$	$z_{\rm CMB}$	Peak MJD	x_1	c	m_B (mag)
PS15bbn	0.037 10 (0.000 12)	0.036 17 (0.000 12)	57213.86 (0.52)	1.57 (0.22)	− 0.064 (0.032)	16.60 (0.06)
PS15bdr	0.070 96 (0.000 01)	0.071 28 (0.000 01)	57215.81 (0.16)	− 2.19 (0.22)	− 0.035 (0.036)	18.33 (0.04)
PS15bif	0.079 37 (0.000 27)	0.078 30 (0.000 27)	57234.06 (0.24)	0.34 (0.30)	− 0.016 (0.034)	18.20 (0.06)
PS15bjg	0.068 89 (0.000 01)	0.067 64 (0.000 01)	57239.11 (0.17)	− 1.16 (0.21)	− 0.101 (0.037)	18.03 (0.07)
PS15brr	0.051 80 (0.000 09)	0.050 51 (0.000 09)	57259.41 (0.02)	0.82 (0.18)	− 0.086 (0.033)	17.00 (0.05)
PS15bsq	0.034 30 (0.000 02)	0.033 55 (0.000 02)	57262.87 (0.12)	0.56 (0.12)	− 0.071 (0.029)	16.26 (0.04)
PS15bst	0.088 50 (0.000 17)	0.087 26 (0.000 17)	57259.26 (1.27)	2.59 (0.65)	− 0.046 (0.049)	18.34 (0.08)
PS15bwh	0.072 67 (0.000 43)	0.071 49 (0.000 43)	57278.96 (0.15)	0.84 (0.19)	− 0.120 (0.030)	17.65 (0.04)
PS15bzz	0.080 24 (0.000 01)	0.079 44 (0.000 01)	57284.32 (0.67)	− 0.89 (0.26)	− 0.015 (0.032)	18.34 (0.04)
PS15cfn	0.110 57 (0.000 15)	0.109 49 (0.000 15)	57310.04 (0.30)	1.23 (0.34)	− 0.080 (0.020)	18.83 (0.03)
PS15cge	0.085 19 (0.000 01)	0.084 18 (0.000 01)	57317.77 (0.10)	1.48 (0.41)	0.409 (0.066)	19.53 (0.10)
PS15cku	0.023 27 (0.000 07)	0.023 57 (0.000 07)	57319.34 (0.24)	0.64 (0.10)	0.008 (0.029)	15.72 (0.04)
PS15cms	0.064 79 (0.000 03)	0.066 52 (0.000 03)	57326.64 (0.19)	1.01 (0.15)	0.013 (0.033)	17.85 (0.05)
PS15cwx	0.030 07 (0.000 11)	0.030 96 (0.000 11)	57348.49 (0.27)	− 1.42 (0.08)	− 0.065 (0.040)	16.18 (0.10)
PS15cze	0.039 37 (0.000 02)	0.040 78 (0.000 02)	57364.41 (0.18)	− 1.62 (0.23)	0.080 (0.042)	17.58 (0.12)
PS15mt	0.070 85 (0.000 09)	0.071 48 (0.000 09)	57105.83 (0.27)	1.45 (0.25)	− 0.087 (0.030)	17.89 (0.04)
PS16amf	0.090 00 (0.006 00)	0.090 58 (0.006 00)	57440.23 (0.27)	2.78 (0.30)	0.127 (0.039)	18.06 (0.08)
PS16cqa	0.043 86 (0.000 01)	0.045 36 (0.000 01)	57545.28 (0.75)	− 2.80 (0.35)	0.171 (0.052)	18.22 (0.08)
PS16drf	0.057 49 (0.000 10)	0.056 01 (0.000 10)	57610.68 (1.48)	− 1.27 (0.50)	0.699 (0.089)	19.46 (0.13)
PS16em	0.069 82 (0.000 17)	0.070 98 (0.000 17)	57386.49 (0.86)	− 0.98 (0.16)	0.181 (0.064)	18.77 (0.10)
PS17tn	0.044 70 (0.000 01)	0.046 07 (0.000 01)	57785.85 (0.12)	− 0.71 (0.11)	0.041 (0.028)	17.31 (0.04)
PS17yt	0.069 76 (0.000 02)	0.070 62 (0.000 02)	57786.90 (0.12)	− 0.20 (0.15)	− 0.139 (0.027)	17.78 (0.04)
PSN J01534240+2956107	0.025 65 (0.000 01)	0.025 63 (0.000 01)	57393.65 (0.10)	− 0.56 (0.08)	0.086 (0.029)	16.22 (0.05)
PSN J02524671+4656470	0.028 09 (0.000 03)	0.028 03 (0.000 03)	57289.71 (0.27)	− 0.16 (0.13)	− 0.080 (0.083)	15.93 (0.21)
PSN J08593491+4555343	0.028 12 (0.000 01)	0.029 27 (0.000 01)	57099.28 (0.15)	− 0.76 (0.10)	0.063 (0.028)	16.51 (0.04)
PSN J12040516+1404059	0.043 85 (0.000 01)	0.045 57 (0.000 01)	57170.32 (0.10)	1.29 (0.17)	0.018 (0.032)	17.07 (0.04)
PSN J16025128+4713292	0.020 25 (0.000 13)	0.020 33 (0.000 13)	57172.44 (0.13)	0.68 (0.08)	0.097 (0.028)	15.68 (0.04)
PSN J16283836+3932552	0.031 19 (0.000 01)	0.031 73 (0.000 01)	57163.85 (0.27)	− 2.39 (0.09)	− 0.022 (0.033)	16.86 (0.04)
PSN J20435314+1230304	0.015 50 (0.000 02)	0.015 06 (0.000 02)	57226.03 (0.17)	− 2.54 (0.15)	0.104 (0.040)	15.71 (0.07)
PSN J23102264+0735202	0.039 15 (0.000 09)	0.038 01 (0.000 09)	57281.19 (0.16)	0.50 (0.16)	0.159 (0.031)	17.38 (0.05)
PSN J23523718+1433092	0.026 48 (0.000 01)	0.026 01 (0.000 01)	57284.00 (0.44)	− 2.01 (0.13)	− 0.011 (0.036)	16.41 (0.05)
iPTF17fs	0.068 00 (0.010 00)	0.068 52 (0.010 00)	57762.57 (1.60)	1.35 (0.57)	0.178 (0.088)	19.27 (0.15)

cosmological subsample is −19.48 mag. Although it is unclear if these objects are truly similar to SN 2006gz, this is a strong possibility. If that were the case, then up to 6.2 per cent of the Foundation Supernova sample is comprised of SN 2006gz-like objects, a surprisingly large number. The large fraction of SN 2006gz-like objects in our sample is likely the result of selecting more galaxies from low-luminosity galaxies, which have a higher relative rate of this class, compared to previous samples (Khan et al. 2011; Taubenberger et al. 2011). Detailed light-curve and spectral analyses should improve our classification for these objects.

Table 7. Sample Cuts

Criterion	No. of SNe not passing	Cum. no. of SNe not passing	SNe remaining
Initial sample	–	–	225
Not similar to SNe Iax, SN 1991bg, or SN 2006gz	12	12	213
$E(B-V)_{\rm MW} < 0.25$ mag	5	17	208
Sufficient LC coverage	3	20	205
$t_{\rm first} < 7$ d	7	25	200
$\sigma(x_1) < 1$	1	25	200
$\sigma(t_{\rm peak}) < 1$ d	7	31	194
$-0.3 < c < 0.3$	11	36	189
$-3.0 < x_1 < 3.0$	2	36	189
Chauvenet's criterion	9	45	180

6 DISCUSSION AND CONCLUSIONS

We have presented the survey strategy/design and first results from the Foundation Supernova Survey. Over the next several years, we will use the PS1 telescope to observe hundreds of SNe Ia at $z < 0.1$. These well-measured light curves will provide precise and accurate distances to these SNe, which in turn will provide a foundation for future SN cosmology analyses.

We have motivated our strategy, stressing that the PS1 system is ideal for this work. In particular, PS1 has already observed all positions north of −30 declination, making late-time template observations unnecessary. The PS1 system is a well-calibrated photometric system (to the mmag level) with a precisely and accurately measured instrument response. We have already observed ∼500 spectroscopically confirmed and ∼3000 photometrically classified high-z SNe Ia (Rest et al. 2014; Scolnic et al. 2017; Jones et al. 2017) with PS1. All PS1 SNe (both high-z and Foundation) will be reduced with a single, well-tested data-reduction pipeline.

Our follow-up strategy is economical, yet still provides excellent light-curve coverage. At our current rate, we can observe ∼140 SNe Ia per year, but we believe that we can increase the rate to 200 SNe Ia per year given additional spectroscopic resources and/or timely publicly announced classifications.

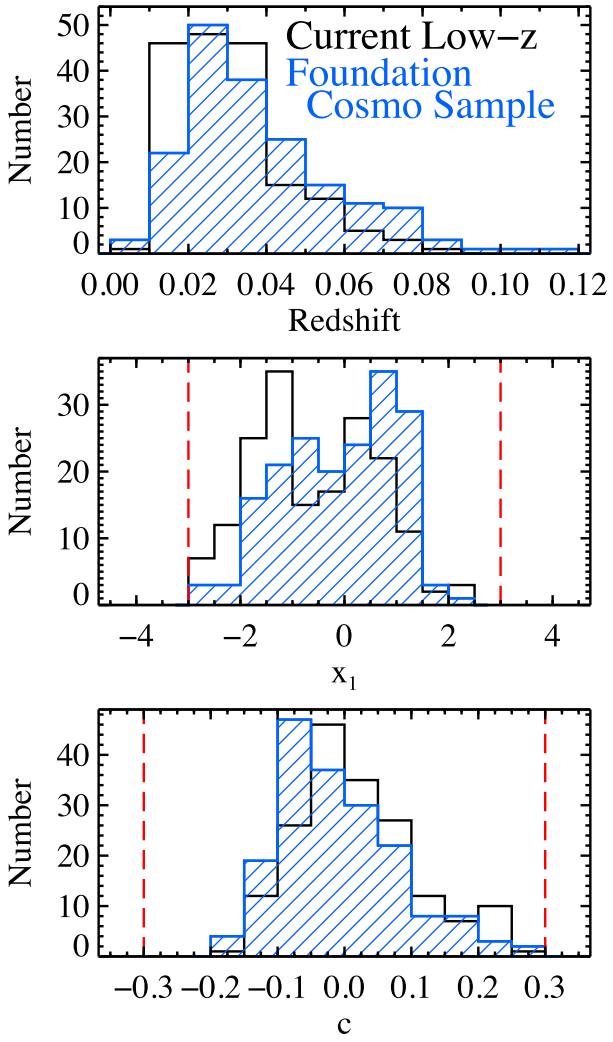

Figure 7. Distributions of redshift (top panel), x_1 (middle), and c (bottom) for the Foundation cosmology (blue hashed), and existing low-z (black) SN samples. The vertical dashed lines correspond to the parameter limits for inclusion in the cosmology sample. The median values for the Foundation cosmology (existing low-z) sample are 0.033 (0.029), 0.048 (0.160), and −0.021 (−0.035), respectively.

We already have obtained 225 complete SN Ia light curves, which we present here (and release publicly). From those data, we have derived light-curve parameters and distance estimates. We created a Hubble diagram for the Foundation cosmology sample of 180 SNe Ia, finding that we have already created a competitive sample that is both larger than every other homogeneous sample of low-z SNe Ia and with low intrinsic scatter ($\sigma_{\rm int} = 0.111$ mag). This sample is already comparable in size to the entire current low-z SN Ia sample used for cosmological analyses.

Our current sample comes primarily from untargeted SN searches (mostly ASASSN and PSST), and a large fraction of SNe Ia have relatively faint host galaxies. One-third of all host galaxies did not have a catalogued redshift, and we provide redshifts here for those galaxies. There are a surprising number of SNe Ia that have Hubble residuals of $d\mu \approx -0.6$ mag. While these SNe are removed from the cosmologically useful subsample through various cuts (and in particular Chauvenet's criterion), these may be peculiar SNe Ia that do not have adequate spectroscopic data to distinguish them from more typical SNe Ia.

In the coming months and years, we will make further improvements to our data reduction pipeline, add host-galaxy and spectral data, and eventually constrain cosmological parameters. We expect our next data release to be larger than the entire current low-z sample.

The Foundation Supernova Survey is critical for the success of current and future surveys such as DES, LSST, and *WFIRST*. As SN cosmology analyses are currently systematics limited and the largest systematic is currently the low-z sample, the Foundation Supernova Survey will have a larger impact on measuring cosmological parameters than the current generation of high-z surveys.

ACKNOWLEDGEMENTS

We thank the SN community, both professional and amateur, for its tireless efforts discovering and classifying SNe. We especially thank those who make discoveries, classifications, and data immediately public. Timely, public access to this information was both critical for this work and a significant benefit for all of science. We especially thank A. Castro-Tirado, R. Chornock, A. Gal-Yam, B. Shappee, I. Shivvers, J. Strader, and O. Yaron for providing additional information about their observations. We thank S. Downing, A. Duarte, M. Garcia, R. Hounsell, A. Kniazev, M. Kotze, B. Miszalski, B. Patel, E. Romero Colmenero, R. Skelton, and J. Tonry for assisting in some of the observations presented here. We thank C. Stubbs for his continued support of this project and other intellectual contributions.

This manuscript is based upon work supported by the National Aeronautics and Space Administration under Contract No. NNG16PJ34C issued through the *WFIRST* Science Investigation Teams Programme. RJF and DS were supported in part by NASA grant 14-WPS14-0048. The UCSC group is supported in part by NSF grant AST-1518052, the Gordon & Betty Moore Foundation, and from fellowships from the Alfred P. Sloan Foundation and the David and Lucile Packard Foundation to RJF. DS acknowledges support from NASA through Hubble Fellowship grant HST-HF2-51383.001 awarded by the Space Telescope Science Institute, which is operated by the Association of Universities for Research in Astronomy, Inc., for NASA, under contract NAS 5-26555 and the Kavli Institute for Cosmological Physics at the University of Chicago through grant NSF PHY-1125897 and an endowment from the Kavli Foundation and its founder Fred Kavli. The research leading to these results has received funding from the European Research Council under the European Union's Seventh Framework Programme (FP7/2007-2013)/ERC Grant agreement no. [291222] (PI: SJS).

Pan-STARRS is supported in part by the National Aeronautics and Space Administration under Grants NNX12AT65G and NNX14AM74G. The Pan-STARRS1 Surveys (PS1) and the PS1 public science archive have been made possible through contributions by the Institute for Astronomy, the University of Hawaii, the Pan-STARRS Project Office, the Max-Planck Society and its participating institutes, the Max Planck Institute for Astronomy, Heidelberg and the Max Planck Institute for Extraterrestrial Physics, Garching, The Johns Hopkins University, Durham University, the University of Edinburgh, the Queen's University Belfast, the Harvard-Smithsonian Center for Astrophysics, the Las Cumbres Observatory Global Telescope Network Incorporated, the National Central University of Taiwan, the Space Telescope Science Institute, the National Aeronautics and Space Administration under Grant No. NNX08AR22G issued through the Planetary Science Division

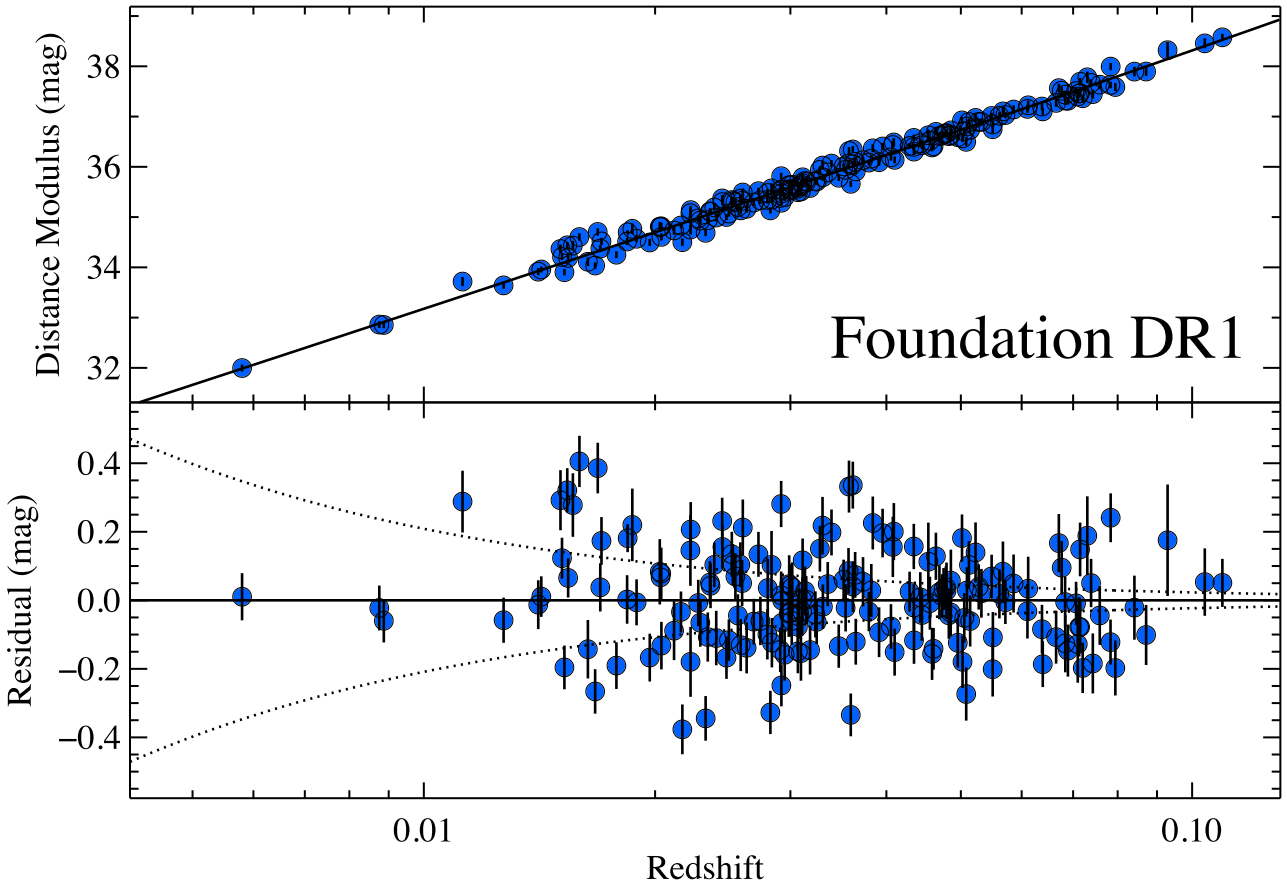

Figure 8. Hubble diagram for the Foundation DR1 sample and residuals to a fiducial ΛCDM model (lower panel). Error bars do not include uncertainties related to peculiar velocities (which are represented by the dotted curves in the lower panel) and redshift uncertainties.

of the NASA Science Mission Directorate, the National Science Foundation Grant No. AST–1238877, the University of Maryland, Eotvos Lorand University (ELTE), the Los Alamos National Laboratory, and the Gordon and Betty Moore Foundation.

This paper is based on observations (NOAO Prop. IDs: 2015A-0253 and 2015B-0313; PI: RJF) obtained at the Southern Astrophysical Research (SOAR) telescope, which is a joint project of the Ministério da Ciência, Tecnologia, e Inovação (MCTI) da República Federativa do Brasil; the U.S. National Optical Astronomy Observatory (NOAO); the University of North Carolina at Chapel Hill (UNC); and Michigan State University (MSU), and at Kitt Peak National Observatory, NOAO, which is operated by the Association of Universities for Research in Astronomy (AURA) under cooperative agreement with the National Science Foundation. The authors are honoured to be permitted to conduct astronomical research on Iolkam Du'ag (Kitt Peak), a mountain with particular significance to the Tohono O'odham.

Some of the data presented herein were obtained at the W. M. Keck Observatory, which is operated as a scientific partnership among the California Institute of Technology, the University of California, and the National Aeronautics and Space Administration. The Observatory was made possible by the generous financial support of the W. M. Keck Foundation. The authors wish to recognize and acknowledge the very significant cultural role and reverence that the summit of Maunakea has always had within the indigenous Hawaiian community. We are most fortunate to have the opportunity to conduct observations from this mountain.

Research at Lick Observatory is partially supported by a generous gift from Google.

Some of the observations reported in this paper were obtained with the Southern African Large Telescope (SALT), and we thank the SALT Astronomers for assistance.

Based on observations obtained with the Apache Point Observatory 3.5-m telescope, which is owned and operated by the Astrophysical Research Consortium.

We acknowledge use of some data collected at the European Organisation for Astronomical Research in the Southern Hemisphere, Chile as part of PESSTO, (the Public ESO Spectroscopic Survey for Transient Objects Survey) ESO programme 188.D-3003, 191.D-0935.

This manuscript was initiated during the 'Dynamic Universe: Understanding ExaScale Astronomical Synoptic Surveys' workshop at the Aspen Center for Physics, which is supported in part by the NSF under grant No. PHYS-1066293. RJF and DS thank the Aspen Center for Physics for its hospitality during the 'Dynamic Universe' workshop in 2015 June.

Facility: Pan-STARRS-1 (GPC1); SOAR (Goodman spectrograph); Mayall (KOSMOS spectrograph); FLWO:1.5m (FAST); ARC (DIS); SALT (RSS); Keck:I (LRIS); Keck:II (DEIMOS) Shane (Kast)

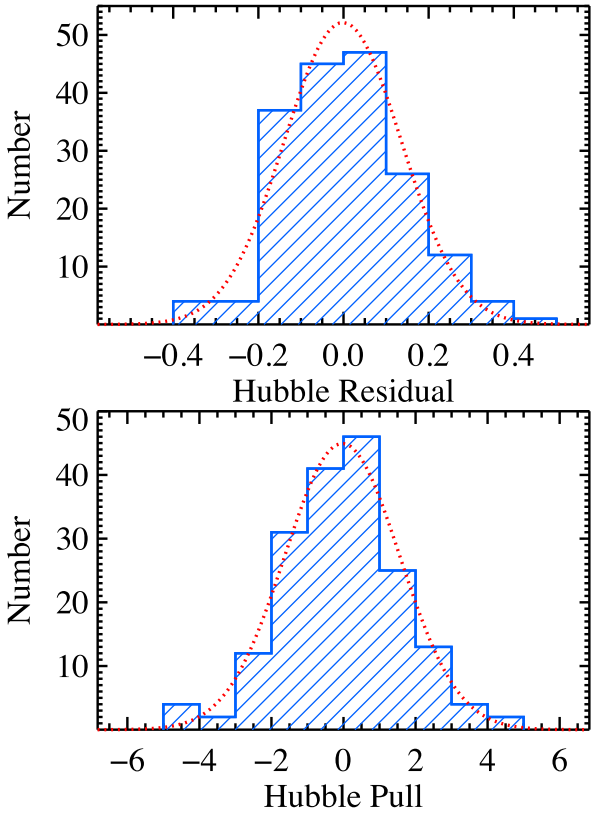

Figure 9. Distributions of Hubble residuals (top panel) and pulls (bottom panel) for the Foundation DR1 cosmology sample. The red dotted curves represent best-fitting Gaussian functions to the distributions. The best-fitting Gaussian functions have standard deviations of 0.138 mag and 1.60 for the Hubble residuals and pulls, respectively.

REFERENCES

Alam S. et al., 2017, MNRAS, 470, 2617
Albrecht A. et al., 2006, preprint (astro-ph/0609591)
Anderson L. et al., 2014, MNRAS, 441, 24
Antilogus P., Astier P., Doherty P., Guyonnet A., Regnault N., 2014, J. Instrum., 9, C03048
Astier P. et al., 2014, A&A, 572, A80
Bailey S. et al., 2009, A&A, 500, L17
Barone-Nugent R. L. et al., 2012, MNRAS, 425, 1007
Becker A., 2015, Astrophysics Source Code Library, record ascl:1504.004
Bernstein J. P. et al., 2012, ApJ, 753, 152
Betoule M. et al., 2014, A&A, 568, A22
Blondin S., Tonry J. L., 2007, ApJ, 666, 1024
Blondin S., Mandel K. S., Kirshner R. P., 2011, A&A, 526, A81
Bohlin R. C., 1996, AJ, 111, 1743
Burns C. R. et al., 2011, AJ, 141, 19
Chambers K. C. et al., 2016, preprint (arXiv:1612.05560)
Chevallier M., Polarski D., 2001, Int. J. Mod. Phys. D, 10, 213
Chotard N. et al., 2011, A&A, 529, L4+
Conley A. et al., 2008, ApJ, 681, 482
Conley A. et al., 2011, ApJS, 192, 1
Contreras C. et al., 2010, AJ, 139, 519
Dhawan S., Jha S. W., Leibundgut B., 2017, preprint (arXiv:1707.00715)
Elias-Rosa N. et al., 2015, Astron. Telegram, 8016
Filippenko A. V. et al., 1992, AJ, 104, 1543
Finkbeiner D. P. et al., 2016, ApJ, 822, 66
Folatelli G. et al., 2010, AJ, 139, 120
Foley R. J., 2012, ApJ, 748, 127
Foley R. J., Kasen D., 2011, ApJ, 729, 55
Foley R. J. et al., 2009, AJ, 137, 3731
Foley R. J., Sanders N. E., Kirshner R. P., 2011, ApJ, 742, 89
Foley R. J. et al., 2013, ApJ, 767, 57
Fraser M. et al., 2017, Astron. Telegram, 1021
Freedman W. L., Madore B. F., 2010, ARA&A, 48, 673
Freedman W. L., Madore B. F., Scowcroft V., Burns C., Monson A., Persson S. E., Seibert M., Rigby J., 2012, ApJ, 758, 24
Friedman A. S. et al., 2015, ApJS, 220, 9
Gal-Yam A., Mazzali P. A., Manulis I., Bishop D., 2013, PASP, 125, 749
Ganeshalingam M. et al., 2010, ApJS, 190, 418
Guy J., Astier P., Nobili S., Regnault N., Pain R., 2005, A&A, 443, 781
Guy J. et al., 2007, A&A, 466, 11
Guy J. et al., 2010, A&A, 523, A7+
Hamuy M. et al., 1996, AJ, 112, 2408
Hicken M., Garnavich P. M., Prieto J. L., Blondin S., DePoy D. L., Kirshner R. P., Parrent J., 2007, ApJ, 669, L17
Hicken M. et al., 2009a, ApJ, 700, 331
Hicken M., Wood-Vasey W. M., Blondin S., Challis P., Jha S., Kelly P. L., Rest A., Kirshner R. P., 2009b, ApJ, 700, 1097
Hicken M. et al., 2012, ApJS, 200, 12
Hodapp K. W. et al., 2004, Astron. Nachr., 325, 636
Holoien T. W.-S. et al., 2017a, MNRAS, 467, 1098
Holoien T. W.-S. et al., 2017b, MNRAS, 471, 4966
Holtzman J. A. et al., 2008, AJ, 136, 2306
Hounsell R. et al., 2017, preprint (arXiv:1702.01747)
Howell D. A. et al., 2006, Nature, 443, 308
Hu W., 2005, in Wolff S. C., Lauer T. R., eds, ASP Conf. Ser. Vol. 339, Observing Dark Energy. Astron. Soc. Pac., San Francisco, p. 215
Huber M. et al., 2015, Astron. Telegram, 7153, 1
Jha S. W., 2017, preprint (arXiv:1707.01110)
Jha S. et al., 2006, AJ, 131, 527
Jha S., Riess A. G., Kirshner R. P., 2007, ApJ, 659, 122
Jones D. O. et al., 2017, preprint (arXiv:1710.00846)
Kaiser N. et al., 2010, in Stepp L. M., Gilmozzi R., Hall H. J., Proc. SPIE Conf. Ser., Vol. 7733, Ground-based and Airborne Telescopes III. SPIE, Bellingham, P. 77330E
Kasen D., Woosley S. E., 2007, ApJ, 656, 661
Kelly P. L., Hicken M., Burke D. L., Mandel K. S., Kirshner R. P., 2010, ApJ, 715, 743
Kessler R. et al., 2009, PASP, 121, 1028
Khan R., Stanek K. Z., Stoll R., Prieto J. L., 2011, ApJ, 737, L24
Krisciunas K., Phillips M. M., Suntzeff N. B., 2004, ApJ, 602, L81
Lampeitl H. et al., 2010, ApJ, 722, 566
Leibundgut B. et al., 1993, AJ, 105, 301
Lewis A., Challinor A., Lasenby A., 2000, ApJ, 538, 473
Li W. et al., 2001, PASP, 113, 1178
Li W. et al., 2011, MNRAS, 412, 1441
Linder E. V., 2003, Phys. Rev. Lett., 90, 091301
Lira P., 1996, Master's thesis, MS thesis. Univ. Chile
Magnier E., 2006, in The Advanced Maui Optical and Space Surveillance Technologies Conference
Magnier E. A., Liu M., Monet D. G., Chambers K. C., 2008, in Jin W. J., Platais I., Perryman M. A. C., eds, Proc. IAU Symp. 248, A Giant Step: from Milli- to Micro-arcsecond Astrometry. Cambridge Univ. Press, Cambridge, p. 553
Magnier E. A. et al., 2013, ApJS, 205, 20
Magnier E. A. et al., 2016, preprint (arXiv:1612.05242)
Mandel K. S., Wood-Vasey W. M., Friedman A. S., Kirshner R. P., 2009, ApJ, 704, 629
Mandel K. S., Narayan G., Kirshner R. P., 2011, ApJ, 731, 120
Mandel K. S., Foley R. J., Kirshner R. P., 2014, ApJ, 797, 75
Mandel K. S., Scolnic D. M., Shariff H., Foley R. J., Kirshner R. P., 2017, ApJ, 842, 93
Metcalfe N. et al., 2013, MNRAS, 435, 1825
Miknaitis G. et al., 2007, ApJ, 666, 674
Morrell N., Shappee B., Drout M., Dong S., 2017, Astron. Telegram, 1024
Mosher J. et al., 2014, ApJ, 793, 16
Narayan G. et al., 2016a, ApJS, 224, 3
Narayan G. et al., 2016b, ApJ, 822, 67

Nicholl M. et al., 2016, ApJ, 826, 39
Onaka P., Tonry J. L., Isani S., Lee A., Uyeshiro R., Rae C., Robertson L., Ching G., 2008, in McLean I. S., Casali M. M., eds, Proc. SPIE Conf. Ser. Vol. 7014, Ground-based and Airborne Instrumentation for Astronomy II. SPIE, Bellingham, p. 70140D
Padmanabhan N. et al., 2008, ApJ, 674, 1217
Pan Y.-C. et al., 2014, MNRAS, 438, 1391
Pan Y.-C. et al., 2015a, Astron. Telegram, 7375
Pan Y.-C. et al., 2015b, The Astron. Telegram, 7519, 1
Perlmutter S. et al., 1999, ApJ, 517, 565
Phillips M. M., 1993, ApJ, 413, L105
Piascik A. S., Steele I. A., 2016, Astron. Telegram, 9023
Planck Collaboration XVI, 2014, A&A, 571, A16
Planck Collaboration XIII, 2016, A&A, 594, A13
Polshaw J. et al., 2015, A&A, 580, L15
Rest A. et al., 2005, ApJ, 634, 1103
Rest A. et al., 2014, ApJ, 795, 44
Rheault J.-P., DePoy D. L., Behm T. W., Kylberg E. W., Cabral K., Allen R., Marshall J. L., 2010, in McLean I. S., Ramsay S. K., Takami H., eds, Proc. SPIE Conf. Ser. Vol. 7735, Ground-based and Airborne Instrumentation for Astronomy III. SPIE, Bellingham, p. 64
Riess A. G., Press W. H., Kirshner R. P., 1996, ApJ, 473, 88
Riess A. G. et al., 1998, AJ, 116, 1009
Riess A. G. et al., 1999, AJ, 117, 707
Riess A. G. et al., 2009, ApJ, 699, 539
Riess A. G. et al., 2011, ApJ, 730, 119
Riess A. G. et al., 2016, ApJ, 826, 56
Sako M. et al., 2014, preprint (arXiv:1401.3317)
Scalzo R. et al., 2012, ApJ, 757, 12
Schechter P. L., Mateo M., Saha A., 1993, PASP, 105, 1342
Schlafly E. F. et al., 2012, ApJ, 756, 158
Scolnic D., Kessler R., 2016, ApJ, 822, L35
Scolnic D. M., Riess A. G., Foley R. J., Rest A., Rodney S. A., Brout D. J., Jones D. O., 2014a, ApJ, 780, 37
Scolnic D. et al., 2014b, ApJ, 795, 45
Scolnic D. et al., 2015, ApJ, 815, 117
Scolnic D. M. et al., 2017, preprint (arXiv:1710.00845)
Shappee B. J. et al., 2014, ApJ, 788, 48
Silverman J. M., Ganeshalingam M., Li W., Filippenko A. V., Miller A. A., Poznanski D., 2011, MNRAS, 410, 585
Silverman J. M., Ganeshalingam M., Li W., Filippenko A. V., 2012, MNRAS, 425, 1889
Smartt S. J. et al., 2015, A&A, 579, A40
Smartt S. J. et al., 2016, MNRAS, 462, 4094
Spergel D. et al., 2015, preprint (arXiv:1503.03757)
Stetson P. B., 1987, PASP, 99, 191
Stritzinger M. D. et al., 2011, AJ, 142, 156
Stubbs C. W., Tonry J. L., 2012, preprint (arXiv:1206.6695)
Stubbs C. W. et al., 2007, PASP, 119, 1163
Stubbs C. W., Doherty P., Cramer C., Narayan G., Brown Y. J., Lykke K. R., Woodward J. T., Tonry J. L., 2010, ApJS, 191, 376
Sullivan M. et al., 2010, MNRAS, 406, 782
Suzuki N. et al., 2012, ApJ, 746, 85
Taubenberger S. et al., 2011, MNRAS, 412, 2735
Tonry J., Onaka P., 2009, in Advanced Maui Optical and Space Surveillance Technologies Conference
Tonry J. L. et al., 2012, ApJ, 750, 99
Tripp R., 1998, A&A, 331, 815
Wang Y., 2008, Phys. Rev. D, 77, 123525
Waters C. Z. et al., 2016, preprint (arXiv:1612.05245)
Wood-Vasey W. M. et al., 2007, ApJ, 666, 694
Yamanaka M. et al., 2009, ApJ, 707, L118
Zhang J. et al., 2016, Astron. Telegram, 9025

SUPPORTING INFORMATION

Supplementary data are available at *MNRAS* online.

Table 2. PS1 Photometry.

Please note: Oxford University Press is not responsible for the content or functionality of any supporting materials supplied by the authors. Any queries (other than missing material) should be directed to the corresponding author for the article.

This paper has been typeset from a TEX/LATEX file prepared by the author.